The System for Classification of Low-Pressure Systems (SyCLoPS): An All-in-One Objective Framework for Large-scale Datasets

Yushan Han[1], Paul A. Ullrich[1,2]

[1]Department of Land, Air and Water Resources, University of California, Davis, Davis, CA, USA
[2]Division of Physical and Life Sciences, Lawrence Livermore National Laboratory, Livermore, CA, USA

Key Points:

- The first all-inclusive low-pressure system (LPS) detection and classification framework for climate data and model outputs is proposed
- The framework substantially extends LPS track lengths while improving tropical cyclone detection skills
- The framework is useful to study the frequency, structure, development, wind impact, and precipitation contribution of each type of LPS

Corresponding author: Yushan Han, `yshhan@ucdavis.edu`

Abstract

We propose the first unified objective framework (SyCLoPS) for detecting and classifying all types of low-pressure systems (LPSs) in a given dataset. We use the state-of-the-art automated feature tracking software TempestExtremes (TE) to detect and track LPS features globally in ERA5 and compute 16 parameters from commonly-found atmospheric variables for classification. A Python classifier is implemented to classify all LPSs at once. The framework assigns 16 different labels (classes) to each LPS data point (node) and designates four different types of high-impact LPS tracks, including tropical cyclone (TC) tracks, Monsoon System (MS) tracks, subtropical tropical-like cyclone (STLC) tracks, and polar low (PL) tracks. The classification process involves disentangling high-altitude and drier LPSs, differentiating tropical and non-tropical LPSs using novel criteria, and optimizing for the detection of the four types of high-impact LPS. We compare our labels to those in the International Best Track Archive for Climate Stewardship (IBTrACS) and find that they are in good agreement. TC detection using SyCLoPS produces better tropical cyclone detection skill compared to the previous algorithms. Finally, we demonstrate that the output of SyCLoPS is valuable for investigating various aspects of LPSs, such as the evolution of a single LPS track, patterns and trends in LPS activities, and precipitation or wind influence associated with a particular LPS class.

Plain Language Summary

We create a new objective framework (SyCLoPS) that can detect, track, and categorize different kinds of cyclones (low-pressure systems) in datasets. We use an advanced software called TempestExtremes to spot cyclones globally in ERA5 reanalysis and then use a Python program to sort all cyclones into 16 different groups based their characteristics. We also identify four types of significant cyclone tracks: tracks of tropical cyclones, monsoon systems, subtropical cyclones, and polar lows. The framework can recognize cyclones over high-elevation areas and dry cyclones. It can also efficiently separate tropical low-pressure systems and extratropical (non-tropical) systems using a novel method. We compare our results against existing archives and find that the framework produces objectively tracked tropical cyclones that better match the observations, and the labels given by the framework are in good agreement with those given in the subjective archives. Finally, we show that SyCLoPS can help us understand various aspects of low-pressure systems, like how they develop over time, changes in their activity trends, and their related extreme weather.

1 Introduction

Objective feature detection has emerged as a key tool for detecting and tracking various meteorological features in large-scale datasets, and responds to the growing need for advanced impacts-relevant model and climate data analysis. Researchers give considerable attention to detecting and tracking low-pressure systems (LPSs), or cyclones, which are often drivers for high-impact weather including high winds and extreme precipitation. Some more significant LPSs, such as tropical cyclones (TCs), monsoon lows (MLs) or monsoon depressions (MDs), subtropical cyclones (SCs), and extratropical cyclones (EXs), are commonly tracked using specialized tracking algorithms in reanalysis and climate model outputs to derive their climatology and perform climate projections(e.g., Guishard et al., 2009; Neu et al., 2013; Hurley & Boos, 2015; Roberts et al., 2020). Tropical-like cyclones (TLCs) in the subtropics and the polar region, including Mediterranean hurricanes and polar lows (PLs), are capable of producing significant coastal hazards (Toomey et al., 2022), but more rigorous automated tracking has only occurred relatively recently because of advances in model resolution and observations (e.g., Stoll et al., 2018; Zhang et al., 2021; Stoll, 2022; Flaounas et al., 2023).

TempestExtremes (TE; Ullrich & Zarzycki, 2017; Ullrich et al., 2021) is an all-inclusive, state-of-the-art automated Lagrangian feature tracking software package. It is designed to robustly and efficiently detect, track, and analyze any nodal or areal features in large-scale datasets with user-friendly command lines and using parallelized C++. TE has been optimized for TC detection using geopotential thickness and mean sea level pressure closed contour criteria (Zarzycki & Ullrich, 2017). Bourdin et al. (2022) found that TC detection using TE outperforms other methods for the reanalysis dataset ERA5 (Hersbach et al., 2020). Vishnu et al. (2020) used TE to track monsoon systems (MLs and MDs, or MSs) in the North Indian Ocean across different reanalysis products, and observed high success rates. TE has also been combined with the cyclone phase space (CPS) of Hart (2003), which classifies storms based on thermal wind and thermal asymmetry parameters. For example, Zarzycki & Ullrich (2017) used TE and CPS to track both TCs and post-TCs (EXs) based on LPSs' thermal structure, and detect extratropical transition (EXT). Zhang et al. (2021) used a similar approach to detect Mediterranean hurricanes.

Although TE's algorithms are powerful for LPS detection, when applied standalone they have similar restrictions and drawbacks as other specialized methods. Their main restriction stems from the fact that these algorithms exclusively target a single type of LPS using strict thresholds on physical variables. Consequently, detection criteria need to be quite stringent, and controls like seasonality, topographical masks, and latitudinal bounds are required to avoid polluting the dataset with incorrect detections (i.e., false alarms). With these criteria, tracks often end abruptly at regional or temporal boundaries and are shorter in length than analogs in manually tracked datasets, which means that information from the complete LPS lifespan is not available. While the CPS approach has the ability to classify the thermal structure evolution of an LPS throughout its lifetime, it is not designed for LPS classification, as different types of LPS often share similar thermal structures. For example, mature TCs, some post-TCs, EXs experiencing warm seclusion, and some subtropical or hybrid cyclones can all be categorized as shallow or deep symmetric warm-core systems according to the CPS (Hart, 2003). Hence, warm/cold core criteria are likely insufficient to effectively classify global LPSs.

Instead, we propose a new objective framework, called the System for Classification of Low-Pressure Systems (SyCLoPS), to detect, track, and classify all non-negligible LPSs worldwide at once, without any spatial or seasonal limitations. We test our framework in ERA5, and focus exclusively on surface-level LPSs (so upper-level disturbances and lows are out of our scope). The detection and tracking are completed using TE commands, and the classification is done in a separate Python classifier that assigns 16 different types of LPS labels/classes (TD, TC, ML, EX, SC, PL, etc.) and 4 types of high-impact LPS tracks, which are TC Track, MS Track, and two types of TLC Tracks (subtropical TLC and PL tracks). The classification process is based primarily on conventional definitions, observations, and physical (dynamic/thermodynamic) intuition, and is simplified to the extent possible. The atmospheric variables used for classification are commonly found in reanalysis and climate model outputs. Basic machine learning techniques and mathematical optimization are used to refine our thresholds against archives of observed and subjectively identified LPSs. The resulting framework involves only thresholds on basic meteorological fields and includes no "black box" elements.

This new framework produces considerably extended LPS track lengths because of the low detection threshold. The labeled LPS nodes can be compared to the subjective LPS status (labels) in the TC observation archive IBTrACS (Knapp et al., 2010). Labeled tracks is also comparable to subjective TC, MS, and TLC track archives. The framework maintains or improves LPS detection skill without implementation of the above-mentioned restrictions. For example, other TC detection frameworks will often pick up some stronger warm-core extratropical or subtropical systems that were not recorded in IBTrACS even if latitudinal bounds were enforced(Bourdin et al., 2022). The new al-

gorithm addresses this problem, leading to a noticeable increase in TC detection skill without further post-processing.

The manuscript is structured as follows. Section 2 summarizes all the datasets we use to verify our classification thresholds and LPS detection skills. Sections 3-5 explain the general detection and classification processes and justify each of the conditions we set for classification. In section 6, we include some highlights from the classified LPS catalog and discuss potential applications from the SyCLoPS framework. Section 7 concludes the paper and addresses known limitations.

2 Data

We detect, track, and classify LPSs throughout 1979 to 2022 in ERA5 at 3-hour frequency. ERA5 is used for testing our classification algorithms since SyCLoPS includes small or mesoscale features like early-stage TCs and TLCs, which require finer data resolution. Although SyCLoPS is developed using ERA5, it uses a small number of commonly output meteorological fields and so is intended to be applicable to other global or regional meteorological datasets. Additionally, alternative paths are identified if some data or fields are unavailable in regional models or at certain pressure levels. SyCLoPS uses TE's closed contour (hereafter, CC) criteria as much as possible since the CC criteria are designed to be insensitive to model resolution (Ullrich & Zarzycki, 2017). Positive (negative) CC criteria use graph search to make sure that all paths along the unstructured grid in a field from a field's local maximum (minimum) lead to the greatest possible decrease (increase) before reaching a specified great-circle distance (GCD). A list of ERA5 variables used in SyCLoPS is given in Table S1 of supporting information (SI).

To verify detection skill for the four selected types of LPS, we use four subjective datasets for verification. TCs are verified against the widely-used IBTrACS. However, only 3510 main-type tracks that reach 34 knots (17.5 m s^{-1}) from the period of 1979-2021, inclusive, are kept for verifying TC detection skills in IBTrACS. We refer to this dataset as IB-TC. For MSs, we use the Sikka archive Sikka (2006), which provides manually-identified North Indian Ocean monsoon system positions on historic surface weather maps at daily frequency, digitized by Hurley & Boos (2015). Few subjective datasets are available for the two types of TLCs we wish to detect. Elsewhere in the literature, subtropical TLCs (STLCs) may be referred to as subtropical storms (SSs), which is regarded as the most intense category of SCs (Evans & Braun, 2012). Mediterranean TLCs (hurricanes) may be viewed as being among global STLCs, and they are perhaps most well studied, with relatively more observational data available. However, existing subjective datasets for Mediterranean TLCs are still very incomplete. To reconstruct a more credible subjective archive for Mediterranean TLCs or STLCs, we obtain the subjectively tracked data from Flaounas et al. (2023), wherein trained meteorologists identify and track Mediterranean cyclones, including TLCs and other noticeable systems in the region, using ERA5's mean sea level pressure (MSLP) field. We then use the cyclone information table provided in Flaounas et al. (2023) and two online sources (see Open Research section) to select tracks that can be potentially classified as TLCs, while avoiding weaker systems. We also observe that IBTrACS contains a few subtropical storm records, which agencies tend to record when they have the potential to transform into TCs. However, these records are largely incomplete and can often be confused with weaker TCs, so we do not separate them from TC records. For PLs, we use the well-known STARS (Sea Surface Temperature and Altimeter Synergy for Improved Forecasting of Polar Lows) archive (Noer et al., 2011), which includes 185 subjectively identified polar lows from 2002-2011 in parts of the Nordic Seas. Of course, this is also not a complete list of all the PLs in this region due to insufficient observations.

In our objectively tracked LPS dataset, we match our tracks to the tracks in each subjective dataset using different matching algorithms, described in SI text S1. To avoid misclassification of MSs, we also use an objectively tracked North Atlantic easterly wave (EW) dataset (Q. A. Lawton et al., 2022) to construct a corresponding surface LPS dataset (also see SI text S1). These matched TC, MS, STLC, PL, and EW datasets are later used in the classification and data analysis process.

3 The Overall Workflow

MSLP is the starting point for our LPS node detection. Although prior research has also employed 850 hPa vorticity or streamfunction fields to detect monsoon systems or cyclones (e.g., Hodges, 1994; Hurley & Boos, 2015; Vishnu et al., 2020), we consider MSLP a preferable variable for two reasons: (1) local minima/maxima of MSLP are widely used in meteorological agency operations to locate surface pressure systems, including LPSs in IBTrACS; and (2) there is a global agency consensus on the definition of MSLP (Knapp et al., 2010). Further, low-level vorticity or streamfunction data may not be directly available in many datasets when intersecting with the surface, and they have opposite signs for cyclonic systems in the North and South Hemispheres, which could lead to tracks across equatorial regions becoming disconnected if they are not detected and tracked twice using different signs. These factors all contribute to the computational burden of detecting LPSs globally without spatial limitations.

MSLP signals may be generally weaker in the tropics, which makes it difficult to differentiate some weaker LPSs associated with tropical waves. To capture these features in the tracker, we consider the lowest reasonable detection threshold. Namely, an LPS node is flagged at a local minimum MSLP if the MSLP value is lower than the surrounding by at least 10 Pa (0.1 hPa) within 5.5° GCD (a 10-Pa delta positive CC criterion). Although we find this is an extremely low threshold, very weak EWs (particularly those over land) that don't have the minimal surface closed MSLP contour will not be detected.

The pointwise feature detection is performed using the *DetectNodes* function in TE. Besides the MSLP CC criterion, we also require that nodal candidates located within 6° GCD of each other merge into a single node, preserving the one with the lowest MSLP value by specifying the argument `--mergedist "6.0"`, which aligns with the specification in Zarzycki & Ullrich (2017). *DetectNodes* also computes 15 parameters (data columns) directly from input variable fields that are later utilized in the LPS classification process. A summary of those data columns and their abbreviations is included in Appendix A. Please refer to SI Text S5 for a brief explanation for the selection of specifications in the parameters. To construct LPS tracks, we then employ the *StitchNodes* function, which requires the following specifications to connect consecutive nodes in time and form non-negligible LPS tracks (all the TE command details are available in Appendix C):

1. `--mintime "18h"`: LPSs must at least sustain for a time span of 18 hours (equivalent to 7 three-hourly time steps in TE) to avoid too many weak, short-lived, diurnal lows.
2. `--range "4.0"`: Node candidates in two consecutive time steps must be located within 4° GCD distance of each other. This specification is chosen based on the fact that the translation speed of the fastest EXs rarely go over 40 m s^{-1}, or about 140 km per hour (Bernhardt & DeGaetano, 2012; Lodise et al., 2022).
3. `--maxgap "12h"`: A maximum allowable gap of 12 hours (equivalent to 5 time steps) within a track is implemented. A longer gap time is not preferred because it may include too many weak diurnal lows.
4. `"--threshold MSLCC,>=,100.0,5"`: To exclude negligibly weak LPS tracks, a track must contain at least 5 time steps during which MSLP includes a closed contour of depth 100 Pa over a 5.5° GCD (MSLCC $\geq$ 100 Pa) distance from the candidate node.

A total of 7,781,105 data points (nodes) and 379,301 distinct tracks are identified in the 44-year period from 1979 to 2022. The whole tracking process takes about 2 hours using 2 NERSC Perlmutter nodes (each with 128 threads). This forms the input (LPS) catalog for classification, structured in accordance with our description in Appendix A. Subsequently, we employ Python classifier codes (available via Zenodo, see the open research section) to classify each LPS node and assign them labels from the 16 distinct classes, following the workflow illustrated in the accompanying flowchart (Fig. 1). We call the output of this classification workflow the classified (LPS) catalog. The structure of this catalog can be found in Appendix A. Both catalogs are available for download via Zenodo. All the required TE command lines for this framework are printed in SI text S6 and via Zenodo.

Note that we use the LPS catalogs mainly for testing our classification conditions, so the provided catalogs may not be the most comprehensive global LPS dataset considering the data scalability and computation workload. Our detection specifications should be enough for general high-impact LPSs; however, some very small and short-lived high-impact systems, such as some PLs, can be missed because of the 3-hourly detection rate, the 18 hour `mintime`, or the rather large `mergedist`. For these cases, users may select their own regions and LPS features of interest and run *DetectNodes* and *StitchNodes* with alternative specifications before performing classification.
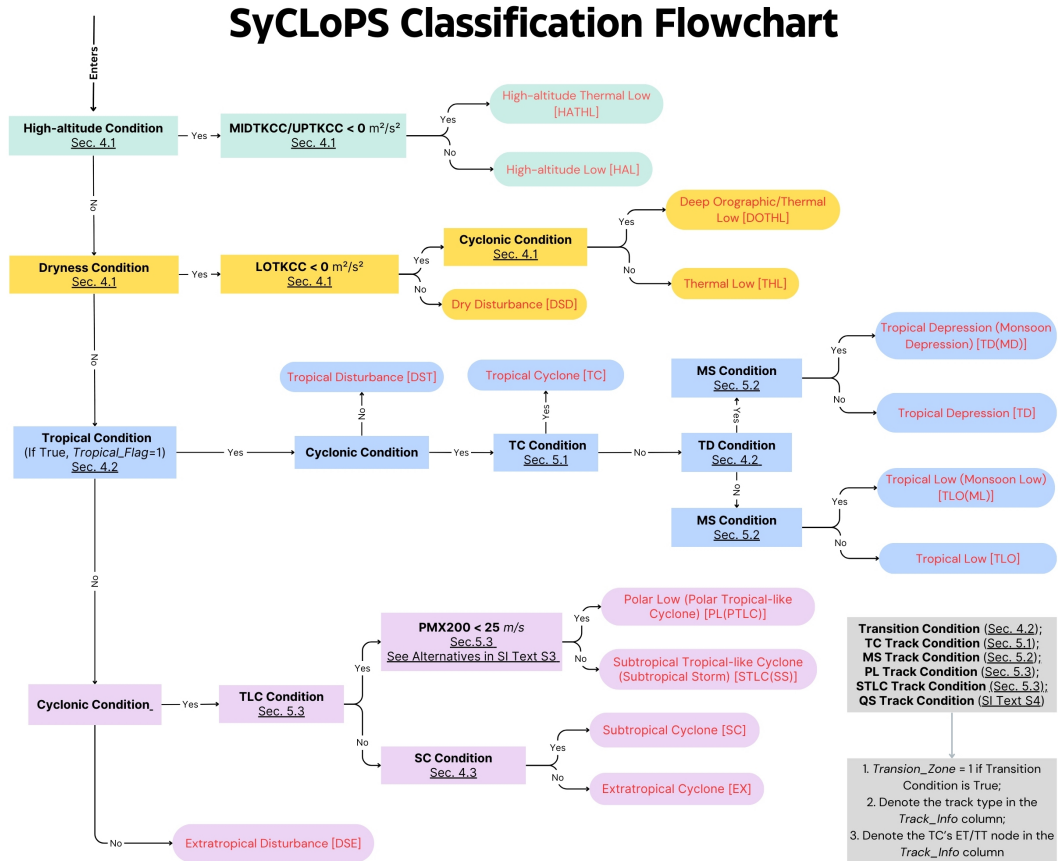

Figure 1. A depiction of the LPS classification workflow. The workflow begins in the top-left. A complete list of parameters is given in Appendix A, and a complete list of conditions is provided in Appendix B. Section numbers are noted in the figure below each condition to indicate where details can be found in the text.

Figure 1 shows the LPS classification flowchart. The workflow flows from top to bottom through five major branches to disentangle each major class of LPS. Boxes with red text indicate the final LPS classification labels (full labels and short labels). Details of the conditions applied in the flowchart can be found in Appendix B. The first branch (green) is the high-altitude branch, where we apply the high-altitude condition to extract those LPSs with a surface elevation higher than the 850 hPa (typically around 1500 m) from the input catalog, given that most of the more influential LPSs occur at a lower altitude. Although not as important, some of these high-altitude lows can be major contributors to precipitation over or near global plateaus (Tucker, 1999; L. Li et al., 2019). The second branch (yellow) is the dry branch. In this branch, we segregate those LPSs that hardly produce any precipitation due to their dry, low-level circulation. This generally includes thermally-driven shallow thermal/heat low systems, which can affect local cold fronts and heat waves (Reeder et al., 2000; Spengler et al., 2005). Third is the tropical branch (blue), which contains several recognizable and impactful features such as TCs, MDs, and MLs. At this level, the remaining unclassified LPSs will be determined to be tropical or non-tropical based on the tropical condition. The fourth branch (purple) is the extratropical branch, where we segregate TLCs (STLCs and PLs) and then differentiate SCs from the most typical EXs.

The gray workflow in the bottom-right of Fig. 1 is used in the second step of the classification. It provides additional useful information for reference purposes, but it does not affect any LPS node labels assigned in the first step: if a track meets a specific track condition using a time step threshold, one or more types of the four high-impact LPS tracks will be labeled in the `Track_Info` column of the classified LPS catalog. For example, if a track with a unique `TID` is determined to be both a "TC track" and "MS track", then in the `Track_Info` column, every node/data point of that track will be denoted "Track_TC_MS." We also introduce the quasi-stationary (QS) track condition that can identify those LPS tracks that stay relatively stationary and bounce around topographic features (see SI Text S3 for information on how we establish the thresholds) so that they can be filtered out or selected when needed. As there's no hard cut-off between a tropical and non-tropical system, we additionally establish the transition condition along with the tropical condition to define a transition zone to address the ambiguity of the more hybrid and marginal tropical systems potentially under transition. The tropical condition must be fulfilled before the transition condition can be justified. The `Tropical_Flag` column and the `Transition_Zone` column in the classified LPS catalog will be set to 1 (or otherwise 0) if an LPS satisfies the tropical condition and transition condition, respectively. Extratropical and tropical transition (EXT and TT) completion nodes are also noted in the `Track_Info` column for TC tracks. We define EXT completion nodes as the first LPS nodes along the track with a non-tropical label after the last tropical-system node, and TT completion nodes as the first TC node before the last non-TC node in TC tracks that originate as a non-tropical LPS or within the transition zone defined in section 4. Users may choose their own standards to redefine EXT and TT positions based on the provided data. Details of the conditions used in the classification process will be discussed further in the next section.

4 Justification for Classification Conditions

4.1 High-altitude and Dry Branch Conditions

In the high-altitude branch, two classes are given based on the mid-level/upper-level warm core criterion (MIDTKCC/UPTKCC). MIDTKCC (UPTKCC) is the negative CC criterion of geopotential thickness between 500 hPa and 700 hPa (300 hPa and 500 hPa) over a 6.5° GCD, from the maximum thickness within 1.0° GCD of an LPS node. Geopotential thickness is used instead of temperature to detect warm cores for the same reasons listed in Zarzycki & Ullrich (2017). Hence, if MIDTKCC or UPTKCC is less than $0 \text{ m}^2 \text{ s}^{-2}$, it indicates that a high-altitude LPS is warm-cored at these levels (same for

the low-level warm-core criterion LOTKCC) and potentially thermally-driven. If this condition is met, the "High-altitude Thermal Low (HATHL)" label will be given; otherwise, the "High-altitude Low (HAL)" label will be used.

The dryness condition determines whether an LPS node will enter the dry branch: It requires that RHAG850 (average 850 hPa relative humidity over a 2.5° GCD) is greater than 60%. This threshold is determined by the lowest track-maximum RHAG850 (the maximum RHAG850 of all nodes within a track) in the matched PL and STLC dataset, chosen to prevent misclassification of significant non-tropical systems in the relatively drier subtropical/extratropical regions. Therefore, we consider RHAG850 at 60% a safe threshold to separate dry convective systems from moist convective systems. Next, the LOTKCC < 0 m^2 s^{-2} criterion is used to examine LPSs' low-level warm cores. If the condition is not met, the node will be classified as a "Dry Disturbance (DSD)"; otherwise, we check the cyclonic condition.

The cyclonic condition uses VOR500 (average relative vorticity over a 2.5° GCD) to determine if an LPS has cyclonic circulation beyond mid-level (500 hPa). A typical heat low is considered to have a dry and warm low-level core and is shallow in nature (Smith, 1986; Hoinka & Castro, 2003). Hence, if an LPS node does not qualify for the cyclonic condition, it will be labeled as a "Thermal Low (THL)." However, some deeper THLs still emerge near elevated topography in the daytime, such as the type II southwest vortex in southwest China (Feng et al., 2016), so the remaining LPSs in the dry branch are labeled "Deep Orographic/Thermal Lows (DOTHL)."

4.2 Tropical Branch Conditions

The next step in the classification framework focuses on tropical systems. Traditionally, tropical systems have been identified using a warm-core criteria (e.g., Zarzycki & Ullrich, 2017; Roberts et al., 2020). However, in the course of this work we found that this criterion is often satisfied outside of the tropics and so lends to many false alarms in the classification. This observation motivated us to examine other fields. We would also like to avoid deterministic temperature thresholds as much as possible since they can be sensitive to global warming, and various types of LPSs can exist over similar sea surface temperatures (SSTs) in the subtropical oceans. Consequently, we found that RH100 (maximum relative humidity at 100 hPa within 2.5° GCD of LPS node) is more reliable and flexible for disentangling tropical and extratropical systems as a proxy of "tropicality." There are two reasons that physically ground this choice. First, RH at 100 hPa is distinctly higher in the tropics. This is because only in the tropics is the tropopause often found above 100 hPa, as a result of active moist convection in the tropics. RH is high there because of the low tropopause temperature and presence of upper-level moisture. RH100 also decreases sharply in the subtropics, reflecting the dynamics of the troposphere and the transition between the tropics and subtropics near the edge of the Hadley cells (see SI Fig. S1 for an illustration of the 1979-2022 global mean RH100). Second, higher RH100 values indicate the presence of deep convection associated with a tropical system, and so this parameter is sensitive to EXT scenarios during which it decreases rapidly while TCs gradually lose their deep convective cores and become post-tropical.

To illustrate the behavior of RH100 during EXT, we examine a recent EXT case (2023 hurricane "Lee") plotted with RH at 100 hPa in Fig. 2. In Fig 2a, the system was embedded in a region of high-level 100 hPa RH two days before EXT completion (between 00-06 UTC, Sep 15) as defined by the National Hurricane Center (NHC). In Fig. 2b, less than one day before EXT completion, the surrounding RH had dropped as the hurricane enters the subtropics. However, a belt of higher RH remains stretched out from the deep tropics, indicating the system's remaining "tropicality." RH100 is still over 90% at this point, as indicated by the bluish color within the 2.5° GCD circle. In Fig. 2c, hours

after EXT completion, we can see that the 100 hPa environment near the hurricane had become warm and dry, leading to a dramatic decrease in RH100.

In addition to RH100, DPSH (average deep-layer wind speed shear between 200 hPa and 850 hPa over a 10.0° GCD) is also used to distinguish tropical systems in the subtropics, especially during EXT. Deep-layer shear is a good physics-related indicator of baroclinicity or an unfavorable environment for tropical deep convection. Post-TCs and general SCs/EXs primarily derive energy from baroclinic sources and are often surrounded by much more intense wind shear compared to tropical systems.
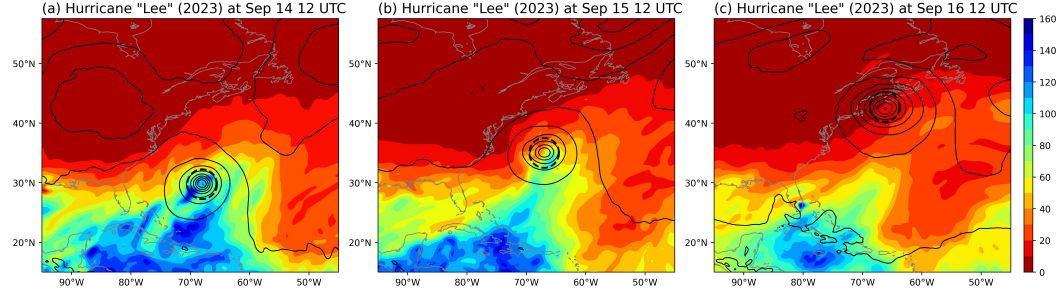

Figure 2. ERA5 Relative Humidity (RH) at 100 hPa during an example of a EXT case (Hurricane "Lee" of 2023) at (a) one day before EXT, (b) during EXT, and (c) soon after EXT. MSLP is shown using black contours. Note that RH at 100 hPa can exceed 100% in some datasets, reflecting supersaturation.

The tropical (and transition) condition with RH100 and DPSH is constructed as follows. First, we use two LPS node clusters that are hard to distinguish from SST or warm-core criteria. One consists of all the matched tropical systems recorded in IBTrACS in the subtropics (the tropical cluster), and the other consists of potential subtropical systems over relatively warm SSTs that are not recorded anywhere in IBTrACS (the subtropical cluster). Note that both clusters (especially the unverified subtropical cluster) will inevitably include some misclassified or transitional LPSs. Details of how we select these two clusters can be found in SI Text S2. We then apply the decision tree classifier over RH100 and DPSH using Gini index splitting criteria to the nodes in the two clusters with a tree depth of 2. Results in Fig. 3 show that the tropical and subtropical clusters can be successfully differentiated by a minimum RH100 threshold of about 20% (rounded off to the nearest 5%) and a maximum DPSH of 10 m s^{-1}. The accuracy score for this decision near 80%. We perform a sensitivity test as demonstrated in SI Text S2 and Fig. S2. These two thresholds are determined to be relatively stable and insensitive to a sensitive standard (the SST requirement) we choose for selecting the two clusters. The elongated outer contours of the tropical cluster towards the left are likely made up of some LPSs near or after EXT/TT (for reference, about 5% of labels in IBTrACS are "Extratropical"), but also some "drier" tropical systems in drier or less convective basins. For example, while only 6 or 0.6% of Western North Pacific (WNP) TC tracks have a track-maximum RH100 under 50%, 94 or 17% of TC tracks in the North Atlantic fall into this range, with 24 tracks falling under 20%. According to these results, the 20% RH100 threshold will serve as the minimum RH100 requirement in the tropical condition, and the 10 m s^{-1} DPSH threshold will be the minimum DPSH requirement in the transition condition, as stronger tropical systems can tolerate a much greater DPSH value, such as in many EXT cases, and DPSH of some weak LPSs closer to the equator can slightly exceed the 10 m s^{-1} threshold due to the tropical easterly jet. The cores of tropical easterly jets at 200 hPa are most commonly found near 5° N to 15° N (Lu & Ding, 1989).

Hence, we impose that the transition condition will not be triggered when an LPS is within 15° latitudes of the equator.
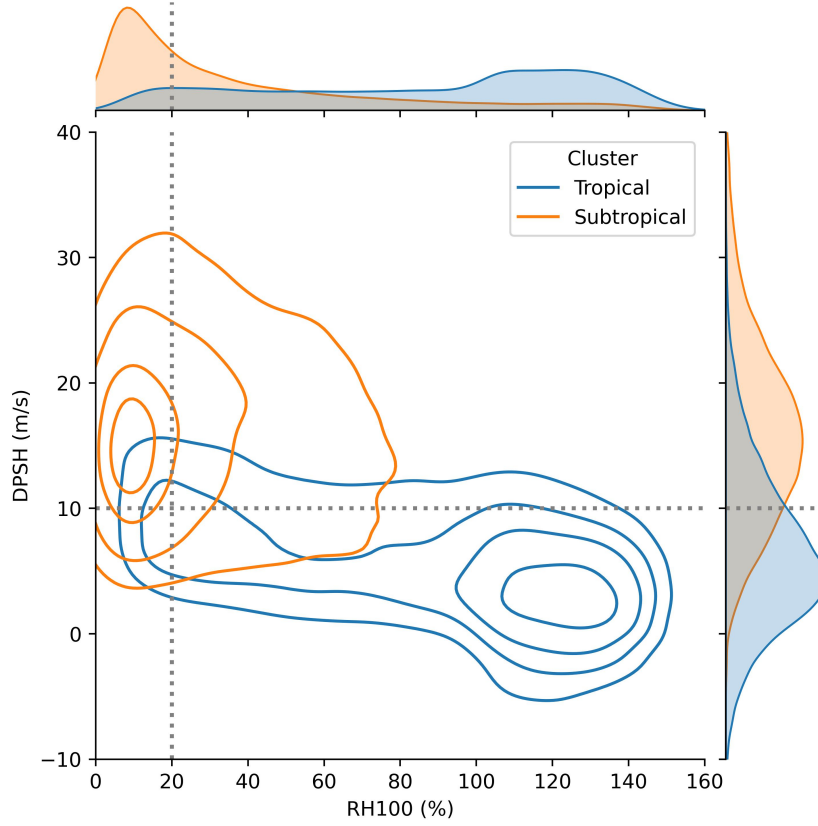

Figure 3. Kernel Density Estimate (KDE) on the RH100-DPSH plane for the tropical cluster and the subtropical cluster. The KDE levels are 0.25, 0.5, 0.75, and 0.9. Grey dotted lines indicate the classification thresholds determined by the decision tree classifier.

To find the upper limit of DPSH for the tropical condition, we select 885 EXT tracks from the matched TC datasets whose pairs in IBTrACS have a "ET (Extratropical)" or "MX (Mixture, contradicting nature reports from different agencies)" label following the last "TS (Tropical System)" label in the `NATURE` column, and here we define the time of the last "TS" label as the EXT completion time of each EXT track. The pre-EXT cluster is defined by those nodes that are 3 to 24 hours before the EXT completion, and the post-EXT cluster is made up of those that are 3 to 24 hours after the EXT completion. We apply the decision tree classifier based on DPSH to find the boundary between the two clusters. With an accuracy score of 64%, the results show that the optimal DPSH threshold to distinguish the two clusters is around 18 ms^{-1}. The accuracy score is not high, but it is to be expected–most TCs gradually transform into EXs, so there isn't a hard cut-off. We do not round off the DPSH threshold to the nearest $5 \, \mathrm{m\,s^{-1}}$ since environmental wind shear typically changes slowly in magnitude along an LPS track. This result is also stable to small changes in the selection of the time range for each cluster.

Finally, we consider 55% as the upper limit of RH100 for the transition condition for three reasons: (1) If we apply the decision tree classifier based solely on RH100 to separate the tropical and non-tropical cluster, the threshold for RH100 will be about 55% with a 74% accuracy score; (2) the median RH100 is about 55% at the time of EXT com-

pletion as defined above, and (3) the median track-minimum RH100 in the matched EW dataset (the matched tropical LPS dataset with the lowest average RH100) is also about 55%. In summary, the tropical condition refers to RH100>20% and DPSH<18 m s^{-1}. Upon fulfillment of the tropical condition, the transition condition is satisfied when RH100<55% or DPSH>10 m s^{-1}, and the latitude is poleward of 15°.

If only the RH100 and DPSH thresholds are included in the tropical condition, we find that a small number of polar systems could also satisfy the tropical condition. As shown in SI Figure S1, polar regions can also feature a relatively higher 100 hPa RH that potentially exceeds the RH100 threshold in our tropical condition. This is mostly the result of persistent darkness during polar wintertime, which allows the upper air temperature to fall to exceptionally low values despite a lack of moisture. On the other hand, DPSH also tends to be quite low in polar regions, as they are not in the main baroclinic zone. However, a plot of the T850 (Air temperature at 850 hPa at the node) distribution for all systems satisfying the RH100 and DPSH thresholds indicates that tropical systems and polar systems are separate from each other by a ~15 K (270 K to 285 K) gap (see SI Fig. S3a). Hence, an additional T850 criteria (T850>280K) is included to further distinguish the two systems. We expect this condition is sufficient even under the most extreme global warming scenarios.

Further down the tropical branch, the cyclonic condition determines whether an LPS is shallow and so should be tagged as a "Tropical Disturbance (DST)." The next step involves the TC condition, which identifies tropical cyclones (TCs). The conditions for this step are obtained by parameter optimization and discussed in section 5.1.

Tropical depressions (TDs) are sometimes referred to as the weakest TCs below the tropical storm category. Therefore, the TD condition requires an LPS to at least have weak upper-level warm cores (UPTKCC<0). We do not require a low-level warm core for TDs as many weaker tropical systems develop a upper-level warm core before a stable low-level warm core is established (Reed et al., 1977; Hunt et al., 2016). We additionally require MSLCC (the greatest positive closed contour delta of MSL over a 5.5° GCD) to exceed 160 Pa, determined by the median LPS node's MSLCC at the IBTrACS track start time of each matched TC track, as agencies tend to start recording LPSs when they are reaching TD intensity. Regardless of whether an LPS satisfies the TD condition, the MS condition is also applied to separate monsoonal and non-monsoonal LPSs. The MS condition is obtained by optimization and discussed in section 5.2. After both the TD and MS conditions have been checked, the classifier assigns one of the four TD and Tropical Low (TLO) labels accordingly, as shown in Figure 1.

4.3 Extratropical Branch Conditions

LPS nodes that do not satisfy the tropical condition are non-tropical (extratropical) systems in the extratropical branch. The cyclonic condition separates "Extratropical Disturbances (DSE)" before they are examined under the TLC condition obtained by optimization. The conditions for identifying TLC labels, which include 'STLC(SS)" and "PL(ETLC)", will be discussed in section 5.2. The remaining LPS nodes will go through the SC condition which follows the general definition of a typical SC–a shallow, warm-cored, non-frontal LPS that features an upper-level cold low isolated/detached from the midlatitude westerlies extending its circulation to the surface in the subtropics (U.S. Navy, 1994; Evans & Braun, 2012). Our SC condition states that an LPS must: (1) have a Z500CC greater than 0 m^2 s^{-2} to satisfy the upper-level cold low characteristic; (2) have a LOTKCC less than 0 to guarantee that the low-level is warm-cored; and (3) have a PMX200 (the maximum poleward 200 hPa wind speed within 1.0° GCD longitude) of greater than 30 m s^{-1} (an effective minimum wind speed for identifying jet streams, see Koch et al. (2006)) to increase the likelihood of the system being equatorward of the polar jet. Since PMX200 might not be reliable in some regional models, alternatives to PMX200 thresholds used

in SyCLoPS are listed and explained in SI Text S4. We do not require EXs to be cold-cored since many Shapiro-Keyser EXs can be warm-cored due to the warm seclusion in their mature stage (Schultz & Keyser, 2021).

5 Criteria Optimization for High-impact LPS Detection

As discussed in section 4, the criteria for TCs, MSs (MDs and MLs), and TLCs all rely on parameter optimization. Since our optimization criteria are based on comparison to subjectively labeled LPS tracks, the parameter optimization procedure also labels LPS tracks by track conditions using the node count parameter (the count of nodes with a specific label within a track) to more stably define an LPS track. Considering that many datasets have a 6-hourly temporal resolution instead of three, the minimum node count we try in this section is 2. We optimize detection skills against different skill metrics discussed below to find the best selected parameter combination upon satisfying conditions upstream of the workflow for each type of LPS. The selection of these parameters is primarily based on physical intuition and previous studies. In this section, we describe the optimization procedure for these four classes of LPS.

5.1 TC Condition Optimization

The TC condition follows the cyclonic condition in the tropical branch. To identify variables for the optimization procedure, we require CMSLCC (the greatest positive closed contour delta of MSLP over a 2.0° GCD) to satisfy some minimum value and UPTKCC to satisfy some maximum value, since TCs are generally characterized by compact MSLP contours and deep warm cores. We choose a CMSLCC criterion over a maximum wind speed criterion because the latter is much more sensitive to model resolution and can be more easily distorted by complex topography. We also demand the node count of TC-labeled nodes within a track to have some minimum value to define a TC track. Evenly spaced values of these three parameters (over 3000 combination) are considered to find the maximum detection skills.

A "test" TC dataset is constructed based on each possible 3-parameter combination for the 1979-2021 period, and it is compared to the reference dataset IB-TC. A "hit" occurs if the test dataset is matched to a track in the reference dataset by appearing within 2° GCD from a reference dataset data point at the same timestamp. A "miss" occurs if a track in the reference dataset does not have a match in the test dataset. A "false alarm" is a track found in the test dataset but are not matched to any tracks in the reference dataset. The TC detection skill metric used here is the hit rate (HR) minus false alarm rate (FAR), expressed as HRMFAR. HR is defined as the ratio of hits to the total number of hits plus misses, and FAR is defined as the ratio of false alarms to the total number of detected/selected tracks.

Figure 4a shows the detection skill of all chosen combinations of the CMSLCC and UPTKCC thresholds, with the optimal node count shown at the top of each combination. The best detection criteria combination found is UPTKCC$<$-107.8$m^2 s^{-2}$ (-11 m), CMSLCC$<$215 Pa (although 210 Pa is also acceptable since it yields near-identical score), and TC-labeled node count $>$8 with HRMFAR reaching 64%. More Details about the TC detection performance are discussed in 6. The CMSLCC and UPTKCC thresholds are used to support the TC condition, and the node step threshold specifies that there must be at least 8 time steps of TC-labeled nodes within a track for the track to be a TC track (the TC track condition).

5.2 MS Condition Optimization

For MS detection optimization under global detection and without seasonal constraints, we demand criteria that could separate MSs from other weaker tropical LPSs,
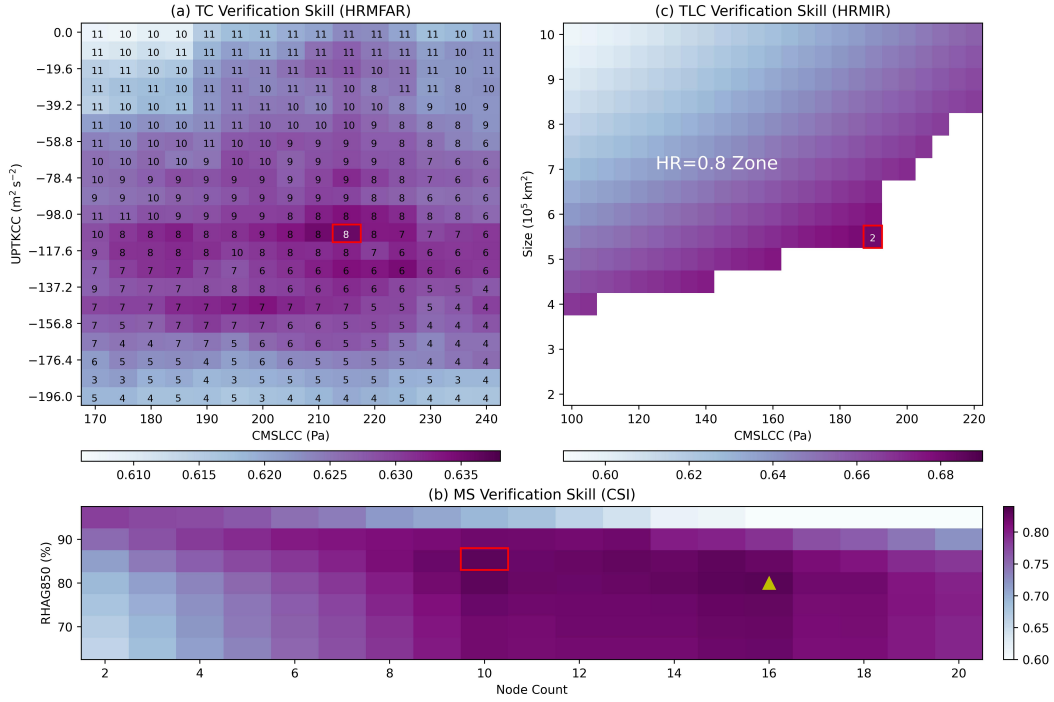
Figure 4. Detection skill optimization for (a) TC, (b) MS, and (c) TLC using different parameter threshold combinations and detection skills metrics shaded by their metric scores. The numbers in (a) and (c) represent the optimized time step for each combination (the optimal node count in (c) is uniform for every combination). The red rectangle in (a) and (b) indicate where the metric scores are maximized and consequently the final thresholds chosen. The metric score shading is only shown for the HR=0.8 zone in (b). In (c), the yellow triangle indicates the maximized score, and the red rectangle marks the final thresholds chosen.

such as EWs. MSs are considered to be born within monsoon troughs as opposed to the intertropical convergence zone (ITCZ) or upper-level easterly waves. According to NHC (n.d.)'s definition, monsoon troughs are characterized by their westerly flow south of the trough, compared to easterly trade winds on both sides of the ITCZ. Furthermore, onsets of regional summer monsoons are often defined as a pattern of a change in wind speed and direction toward stronger westerlies (e.g., Qian & Lee, 2000; Gan et al., 2004). Thus, we develop the UDF850 parameter, which is the difference between the weighted area mean of the positive and negative values of 850 hPa U-component wind over a 5.5° GCD. This allows us to determine whether westerly winds (positive U-component wind magnitudes) or easterly winds (negative U-component wind magnitudes) dominate the local 850 hPa environment of a system. The plot of the UDF850 distribution for the MS and EW matched datasets shows that UDF850=0 m s^{-1} effectively segregates the two clusters (see SI Fig. S3b). Hence, we select UDF850>0 as a minimal requirement for the MS condition.

As implied by the matched MS and EW datasets, MSs in the North Indian Ocean usually have a higher RHAG850 than North Atlantic EWs. This is not surprising, as monsoonal regions are generally considered to have more convective activity and larger moisture transport. Given that Vishnu et al. (2020) also used parameters related to averaged 850 hPa RH to exclude non-monsoon systems, we decide to include a minimum RHAG850 threshold in the MS condition with the threshold undetermined. We compute the Crit-

ical Sucess Index (CSI) as defined below by Vishnu et al. (2020) of all the selected thresh-old combinations to find where CSI is maximal.

$$\text{CSI} = \frac{\text{hits}}{\text{hits} + (\text{misses} + \text{false alarms})/2} \tag{1}$$

A "hit" here is defined as a track in the test dataset having at least one node that is within 3.0° great-circle distance (GCD) of a track point in the Sikka dataset on the same date, and the track must also exist in the matched MS dataset. Since TCs are included in the Sikka dataset and are considered the most intense monsoon systems by the Indian Meteorological Department, tracks that already satisfy the TC track condition and are in the matched MS dataset are automatically considered matched (hits). We apply the detection optimization over the same domain (the North Indian Ocean) and season (June to September) as Vishnu et al. (2020), except that we incorporate the entire available data period rather than just a portion of it. The result shown in Fig. 4c suggests that the maximum CSI reaches 0.83 for RHAG850 = 80% and MS time step = 16. Our best CSI is thus identical to the value found in Vishnu et al. (2020), in support of the framework's ability to detect weaker tropical systems. We finally choose the second highest CSI (also over 0.83) combination, RHAG850 = 85% and MS time step = 10, for the desired thresholds because we would like to include shorter MS tracks. Following these results, the MS condition is set as RHAG850>85% and UDF850>0 m s^{-1}. A node satisfying the MS condition as a MS (TD/TLO) node could be either "TD(MD)" if the TD condition is met at the same time, or "TLO(ML)" if the TD condition is not met. A track is considered to be a MS track only if it has 10 or more MS-labeled nodes. The MS track label highlights those weaker tropical LPS tracks that are more stably labeled as MSs, although they can also coincide with TC-labeled tracks per our standards. Complementary to this, the "TLO" or "TD" label is given if an LPS fails the MS condition as a (non-MS) TD/TLO node. For global detection, weak tropical LPSs associated with EWs, among other types of tropical waves, are likely included in these two categories as well as in other dry or shallow systems/disturbances (i.e., DST and THL). One may make the assumption that weak (non-TCs) tropical (`Tropical_Flag`=1) non-MS LPS nodes in non-MS LPS tracks in some specific regions are (mainly) EWs.

5.3 TLC Condition Optimization

"Tropical-like" refers to LPSs that resemble "real" TCs in certain ways. For instance, a mature Mediterranean hurricane may have a distinct eyewall and a deep warm-core structure despite lower SSTs and greater baroclinity in a non-tropical environment (Pytharoulis et al., 2000). PLs (sometimes referred to as Arctic hurricanes) and Mediterranean hurricanes (STLCs), although still vaguely defined, may all be described as a group of mesoscale (small), intense, and short-lived (in terms of their TLC-stage lifespan) LPSs that can be classified as "tropical-like." The most noticeable difference might be that polar lows are generally defined to develop north of the polar front or the main baroclinic zone in cold air masses(Moreno-Ibáñez et al., 2021), compared to STLCs emerging from the subtropics. The term "hurricane-like extratropical cyclone" is also used in Romero & Emanuel (2017) to group Mediterranean hurricanes and North Atlantic PLs together. Here, we adopt a similar view that STLCs and PLs (which may be viewed as polar TLCs or PTLCs) are comparable to one another but different from the typical EXs/SCs and could be flagged under the same TLC condition. The conventional definition of PLs as being north of the polar front can then be used to distinguish between them. SyCLoPS offers a means for objective global identification of all TLC systems, which includes not only Mediterranean hurricanes and PLs but also the more intense subtropical/extratropical storms worldwide.

Similar parameters, such as CMSLCC and LOTKCC, are used to detect TLCs as we did to detect TCs. We expect TLCs to have, on average, a shallower/weaker warm-

core structure compared to TCs. Hence, we first impose a minimum requirement for the two warm core criteria (LOTKCC<0 and MIDTKCC<0). Static-stability or open-water criteria used in previous PL detection studies (Zappa et al., 2014; Stoll et al., 2018; Stoll, 2022) are not considered here as they appear too restrictive to global TLC detection. For example, PLs may also appear closer to the baroclinic zone in a more sheared environment (Montgomery & Farrell, 1992; Terpstra et al., 2016), and intense storm activity can often occur over Antarctic sea ice (Hepworth et al., 2022). The other significant distinction between TLCs is their small or mesoscale sizes. Thus, we generate LPS size blobs and compute the LOWSIZE parameter conveniently using TE, as described in Appendix C, in addition to the parameters computed by `DetectNodes` to evaluate the extent of LPSs. TE commands with instructions and the Python script for calculating LOWSIZE are provided in SI text S6 and via Zenodo, respectively.

We use the combined matched STLC and PL dataset, which consist of 174 tracks, as our reference dataset for optimization. We concede that it's difficult to evaluate or compare global TLC detection skills because TLCs' records are limited and regional in scope, and their definition inexact. To overcome this, we first remove 12 tracks in the reference dataset that have a track-maximum CMSLCC lower than 215 Pa (the CMSLCC standard for TCs) to further avoid including tracks that are too weak to be considered TLCs. Second, we acknowledge that some TLCs could be embedded within a synoptic-scale circulation or trough in the background, sometimes with a twin low nearby (see SI Fig. S4 for an example)and thus will appear large (or be zero if embedded in a system with lower MSLP) using our size detection method. To work around this observation, we determine that LPSs that have a CMSLCC>420 Pa (90% percentile of detected non-tropical non-shallow LPSs' CMSLCC) and a CMSLCC to MSLCC ratio greater than 0.5 (reflecting that a dominant and more compact LPS core exist within the larger system) are exempt from LOWSIZE requirements. Third, since the scope and quality of the reference dataset is constrained, FAR becomes rather meaningless and is replaced by the infrequency rate (given that TLCs are infrequent), defined as the fraction of selected TLC tracks among all detected tracks that have at least one node that passes the cyclonic condition in the extratropical branch. Hence, the detection skills metric we use for the TLC condition is the HR minus infrequency rate (IR), or HRMIR. Here, HR is simply defined as the fraction of tracks that are detected (hits) in the reference dataset. Given the limited sample size, HR is rounded to the nearest tenth (i.e., 0.750 and 0.849 will be rounded to 0.8) to roughly reflect its 90% confidence interval (CI) and potential sampling errors.

We iterate the selected range of CMSLCC and LOWSIZE threshold combinations for TLC condition optimization. The best HR attained is at the 0.8 level as shown by the shading in the upper left zone of Fig. 4b. Within this zone, the TLC condition is optimal when IR is the smallest (11.9%) at CMSLCC>190 Pa and LOWSIZE<5.5×10^5 km^2 (given that LOWSIZE is nonzero) on top of the other thresholds we mentioned above. The LOWSIZE threshold chosen here agrees with the meso-α scale range (i.e., roughly a 4-500 km LPS radius), which aligns with the upper size range of many studied TLCs (e.g., Holland et al., 1987; Rasmussen & Turner, 2003; Fita et al., 2007). Due to the short-lived nature of TLCs, HRMIR in all combinations maximizes when the node count equals two. LPS nodes that have been tagged as TLC will then be further classified as "PL(ETLC)" or "STLC(SS)" depending on whether they are located further north to the polar jet (PMX200<25 m s^{-1}). Tracks with two TLC-labeled nodes (PL or STLC) and at least one PL (STLC)-labeled node are then assigned PL (STLC) track labels. For an alternative test, we remove the embedded TLC alternate condition and perform the optimization. The results show an identical HR, a slightly lower IR, and 72% overlapped detected TLC tracks when CMSLCC>145 Pa and LOWSIZE<7.0×10^5 km^2. Thus, it may be treated as an alternative TLC condition, although it risks excluding many embedded TLC nodes.

6 Results and Applications

6.1 Main Results

In Fig. 5a, we plot the kernel density estimate (KDE) on the RH100-DPSH coordinate of all 6-hourly-sampled LPS nodes that have passed the second branch and meet the cyclonic condition, to verify the efficacy of our tropical and transition conditions. Our results demonstrate the validity of using RH100 and DPSH thresholds as the foundation for these conditions. The KDE clearly depicts two main clusters, separated by RH100 and DPSH. The solid-line and dash-line boundaries delineate the tropical and transition conditions. The RH100 transition threshold cuts through the narrowest part of the KDE. The cluster centered inside the tropical condition bounds is the tropical system cluster, while the cluster centered outside the box is the non-tropical system cluster, which is apparent from Fig. 5b, where the KDEs of the five matched datasets are placed on the RH100-DPSH coordinate. Within the tropical system cluster, the TC cluster spans the widest range as it includes LPSs undergoing EXT and at post-TC stage, whereas the MS and EW clusters have the highest and lowest mean RH100 values, respectively. Most of the matched tropical LPSs are within the transition boundaries (which may be deemed as the deep tropics). Inside the non-tropical system cluster, the STLC cluster has higher mean DPSH values than the PL cluster. The red filled contours in Fig. 5a depict the KDE of warm-core systems, defined as the previously selected LPS nodes that meet the criterion of UPTKCC<-58.8 $m^2\,s^{-2}$ (-6 m). The KDE shows that warm-core systems can exist in both tropical and non-tropical clusters, and thus, the warm-core criteria may not be ideal for classifying LPSs across the spectrum. According to the classified catalog, the vast majority of the labeled tropical systems are confined within 40 degrees of the equator.
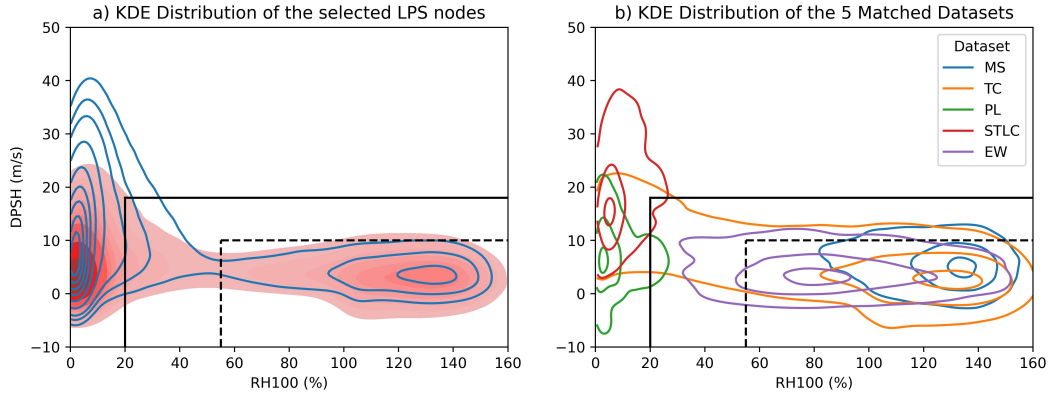

Figure 5. (a) The 10 KDE levels evenly distributed between 0 and 1 of all the selected detected LPS nodes (blue contours) and the warm-core LPS nodes (red filled contours); and (b) the 3 KDE levels set at 0.1, 0.5, and 0.9 of the five matched datasets on the RH100-DPSH coordinate.

SyCLoPS LPS labels are generally in good agreement with the labels in IBTrACS. Two types of labels are provided in IBTrACS: first, the WMO-assigned labels in the `NATURE` column, and second, the labels assigned by US meteorological agencies in the `USA_STATUS` column. The WMO labels are more general than the USA labels, as the USA labels include more classes based on LPSs' intensity. Miscellaneous labels that are vaguely defined and have a small sample size are not included in the comparison. Information about the two agencies' labels can be found on the IBTrACS website and in Landsea & Franklin (2013). Labels are compared when LPS nodes in our dataset and IBTrACS track points
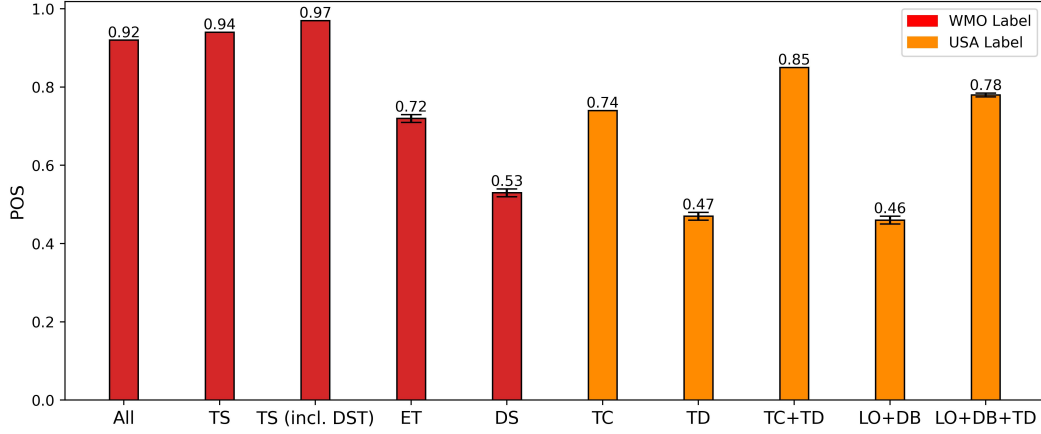
Figure 6. POS of our labels when compared to labels given by WMO (red bars) and USA agencies (blue bars). See text for details. POS values are shown on the top of bars with 95% confidence level error bars denoted.

lie within 2.0° GCD of each other at the same timestamp. 6 shows the probability of success (POS) for correctly labeling an LPS node of a particular class (setting IBTrACS labels as ground truth). Overall, 92% of the matched nodes are in agreement with the WMO labels, mainly contributed by the high "TS" POS of 94% (WMO's "TS" label refers to "tropical system"). Since WMO's "DS (disturbance)" label also exists, we regard "TS" as all non-shallow tropical systems, which is equivalent to all TC and TD/TLO labels in our labeling system. If all our labeled tropical LPSs are considered "TS", the POS increases to 97%, suggesting that very few tropical systems are mistakenly labeled as non-tropical systems by our classification. The extratropical system (EX, SC, STLC, and PL) POS is at 72% when compared to the "ET (extratropical)" label of WMO. The majority of the extratropical records in IBTrACS are post-TCs immediately after EXT. Therefore, it suggests a rather small error in the EXT completion time justified by our classification when compared to IBTrACS. Breaking down the tropical systems, our TC POS remains at a relatively high level of 74% against TC labels given by USA agencies, while TD has a much lower POS of 47%. We find that TDs (TD and TD(MD)) are almost equally likely to be misclassified as TC and TLOs (TLO and TLO(ML)), which reflects ambiguity in their definitions and inevitable biases in LPS intensity evaluations by agencies, reanalysis, and our classification. If TDs are considered a category of TCs for both our labels and IBTrACS's, the POS of "TC+TD" rises to 85%. The weakest system labels in IBTrACS, including LO (low) and DS/DB (disturbance), are more vaguely defined. They are often used at the start of TC tracks, and the labeled LPSs may not have a discernible surface center (Landsea & Franklin, 2013; NHC, n.d.). Hence, we treat them as the same label, which is equivalent to TLOs, DS (DST, DSD, and DSE), and THL (THL, DOTHL, and HATHL) in our labeling system. POS of about 50% is realized for this category compared to labels of WMO and USA agencies. Similarly, they are subject to biases in intensity evaluations and their exact definitions. If TDs are included in this class for both our labels and IBTrACS's, the POS increases to 78%.

TC detection skill is improved using SyCLOPS when compared to the previous TE algorithm (Zarzycki & Ullrich, 2017, the ZU method;). For the ZU method, TC tracks are identified when nodes in a track that satisfy UPTKCC<-58.8 m^2 s^{-2} (-6 m), MSLCC>200 Pa, WS (maximum wind speed at 10 m within 2.0° GCD)>10 m s^{-1}, and ZS<150 m^2 s^{-2} are detected for at least some certain time steps equatorward of 50° latitude. The HRM-FAR of SyCLOPS is the same as the optimal HRMFAR mentioned in 5.1 after we re-
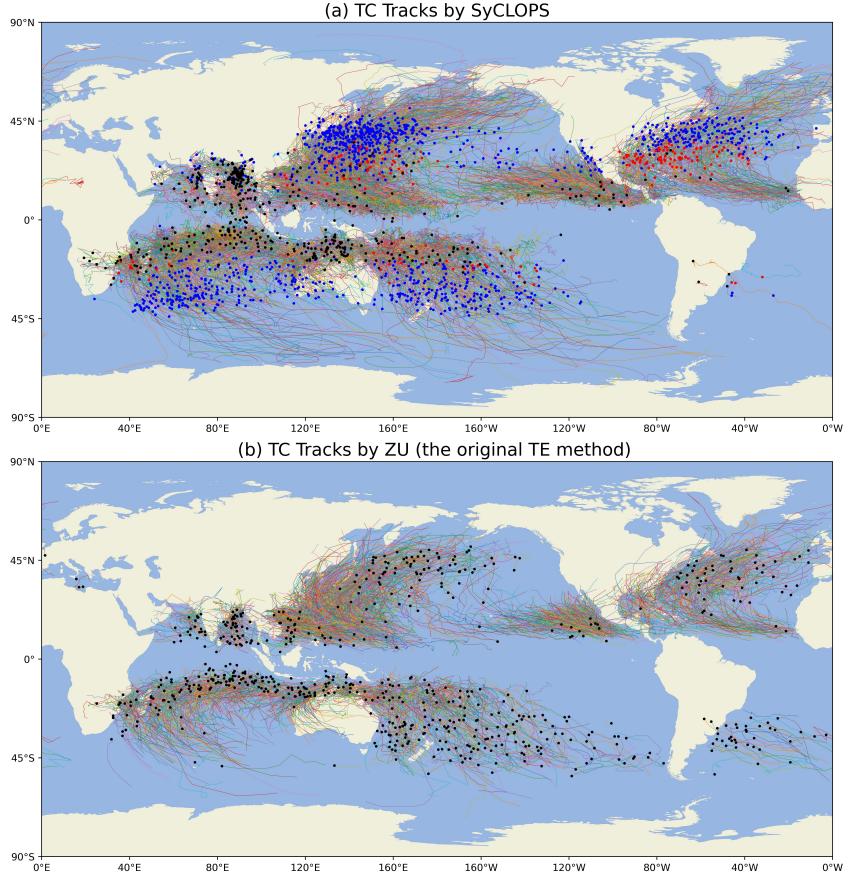
Figure 7. 1979-2021 TC tracks as tracked by (a) SyCLOPS, and (b) the ZU method. Black dots are the first locations of false alarm tracks. Blue and red dots are EXT and TT completion locations indicated by SyCLOPS. 1259 EXT cases and 195 TT cases are detected.

Table 1. Detection skill comparison between SyCLOPS and the ZU method

Method	HR	FAR	HRMFAR	Mean start time difference (hr)	Mean end time difference (hr)
ZU	76.2%	20.1%	56.1%	28	-30
SyCLoPS	78.2%	14.6%	63.6%	-49	30

sample the dataset at a 6-hourly frequency to match the frequency of ZU. The HRM-FAR of ZU is computed against the same IB-TC for the period of 1979-2021 using the same definition of hits and false alarms mentioned in 5.1. Table 1 summarizes the TC detection skill metrics of both methods. The mean start (end) time differences in the table refer to the time differences between the start (end) time of the detected TC track and the corresponding IB-TC track's start (end) time. To summarize, the detection skill improvements are: (1) HRMFAR is increased by 7.5% due to a 5.5% decrease in FAR and a 2% increase in HR; and (2) the early detection of the pre-TC stage and late detection of the post-TC stage are significantly improved, extending TC track length by an average of 137 hours. The effects of these improvements are revealed in Fig. 7. Tracks detected using SyCLOPS are visibly longer at both ends (the pre-TC stage and the post-TC stage) compared to those tracked by ZU. Notably, the new approach more closely

matches IBTrACS observations in the South Atlantic and the Southeast Pacific, among other subtropical oceans, by largely reducing false alarms in those regions. We also notice that many official wind data in IBTrACS's tracks are missing in earlier years in basins of the Indian Ocean (so they are not included in IB-TC) due to the fact that some agencies did not accept their regional responsibility until the early 1990s. Hence, many false alarms in the tropical Indian Ocean for both methods could actually be real TCs (hits). Discrepancies in wind measurement standards, observations, and operational procedures among agencies for different basins are also noted in Schreck et al. (2014), suggesting the presence of a "TC gray zone" due to these biases – i.e., a range of parameter values where different experts would draw different conclusions on the classification of a feature. Therefore, perfectly matching a subjective TC dataset is likely impossible. The blue and red dots show the EXT and TT completion positions of applicable TC tracks. 39% of the identified TC tracks undergo EXT, which is consistent with the global EXT fractions reported in Datt et al. (2022). The new method's HRMFAR may be further elevated through post-processing operations such as eliminating QS tracks or marginal TC tracks that primarily reside in the transition zone. We advise being cautious when eliminating any marginal TCs since they can reside in the "TC gray zone." As an example, the 2001 Australia "Duck" is a classic marginal (debatable) TC (see Garde et al., 2010). Although this storm was not recorded by the agency and it does not satisfy our TC track condition, it is labeled as "TC" at four timesteps under our classification. See SI Fig. S8 for a labeled track map of this special case.
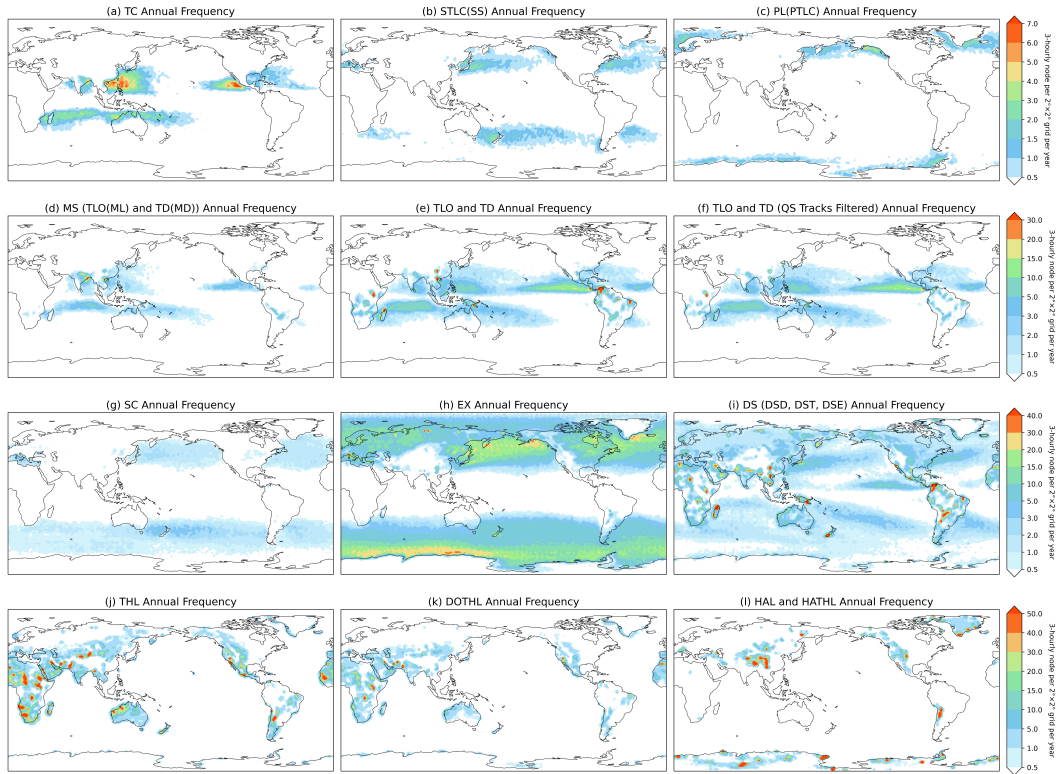

Figure 8. 1979-2022 annual frequency of (a) TC, (b) STLC(SS), (c) PL(PTLC), (d) MS (TLO(ML) and TD(MD)), (e) TLO and TD, (f) TLO and TD with QS track nodes filtered, (g) SC, (h) EX, (i) disturbances, (j) THL, (k) DOTHL, and (l) high-altitude LPS nodes per $2° \times 2°$ grid.

Major globally detected LPS annual frequencies for the different classes of LPSs are shown in Figure 8. In general, the frequencies of these systems are in accordance with observations. Please refer to SI Fig. S5 for a frequency bar plot of all LPS classes. The first row of Fig. 8 contains the least frequent LPS classes, followed by MS in the second row, which are all high-impact LPSs that can be considered extremes. TC frequencies are consistent with their track activity in the tropics and before EXT (Fig. 8a). In Fig. 8b, STLCs/SSs are more frequent in the Mediterranean Sea, the most studied hotspot for these features. They are also commonly found in the storm-track regions (the WNP and the northwestern Atlantic, as defined in Blackmon et al. (1977)), the southwest Atlantic, the southeast Pacific, the Japan Sea, and the Tasman Sea close to Southeast Australia. Those regions are all well known for their intense or tropical-like LPS activities, which include Australian east-coast cyclones, Chilean storms, Japanese south-coast explosive cyclones, TLCs/mesocyclones in the Sea of Japan and the Yellow Sea, and subtropical storms across the Atlantic (see e.g., Heo & Ha, 2008; Guishard et al., 2009; Iwao et al., 2012; Winckler et al., 2017; Gozzo et al., 2014; Shimada et al., 2014; Cavicchia et al., 2018). We expect that successful classification of STLCs is effective for reducing TC false alarms in our framework. PL activity reaches as far south as the Sea of Japan, and they are most prevalent in the Nordic Seas, the Gulf of Alaska, and over or near the sea ice of the Southern Ocean (Fig. 8c). Intense post-TCs are sometimes classified as TLCs, and removing them has only a minor impact on the frequencies of STLCs and PLs. MSs are mainly constrained in the tropical monsoon region defined in (J. Li & Zeng, 2003) and have two evident hotspots in the North Indian Ocean and near the Gulf of Tonkin in the South China Sea (Fig. 8d). Other TLOs and TDs are found throughout the tropics, with some overlap with MS activity and evidence of QS tracks shown by localized high frequencies mainly near rainforest regions (Fig. 8e). After filtering those QS tracks labeled by the QS track condition, strong LPS occurrences largely disappear, leaving other features mostly untouched. SCs are more widespread but less concentrated compared to STLCs (Fig. 8g). EX is the most common type of LPS labeled, and it is omnipresent outside of the tropics (Fig. 8h). Disturbances are found globally across latitudes, and THLs and DOTHLs are located primarily on arid lands. Finally, high-altitude LPSs occupy mountainous areas, including parts of the Antarctic continent.

We show the vertical cross section composites at the latitude of LPS's center for the six selected LPS classes in Figure 9. TCs feature a classic dumbbell-like structure resembling the shape of a cumulonimbus, as indicated by the two RH maxima at the lower- and the upper-level (Fig. 9a). Diabatic heating or latent heat release in TCs, as suggested by the cyclonic potential vorticity (CPV) contours, is evident throughout the lower-level and upper-level. The deep warm-core structure suggested by the potential temperature contours is most evident in the TC composite. Fig. 9b shows that a typical THL features a classic warm and dry low-level core, which is largely constrained to the boundary layer. As shown in Figures 9c and d, weaker tropical systems have far less developed convection and warm cores compared to TCs. MSs have comparatively higher RH at each level and a slightly more developed lower-level circulation than the other weaker tropical LPSs. An eastward tilt of the RH field below 300 hPa is noticeable in the non-MS weak tropical LPS (TD and TLO) composite in Fig. 9d. CPV contours stretching down from the subtropical tropopause in the STLC composite (Fig. 9e) imply that some STLCs undergo a downward development pathway, extracting CPV from upper-level PV anomalies or PV streamers, which agrees with the Mediterranean hurricane development mechanisms described in Flaounas et al. (2022). The warm core and the diabatic heating are more constrained to the lower level for PLs, as depicted in Fig. 9f. Despite the fact that both TCs and TLCs (STLCs and PLs) have relatively deeper warm cores, the upper-level RH of STLCs and PLs is significantly lower than that of TCs and other tropical systems. This distinction supports our choice of the RH100 criterion in the tropical condition.
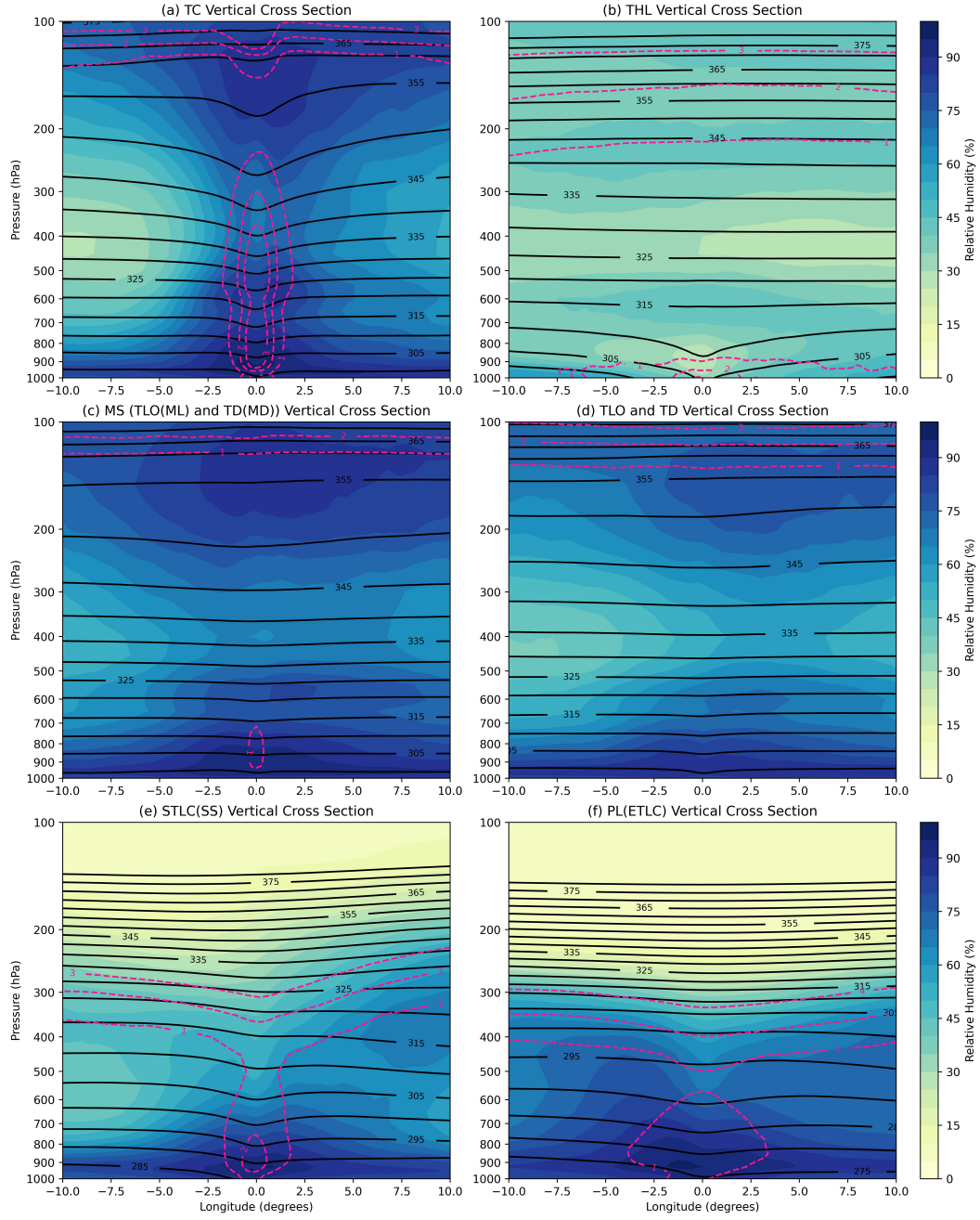
Figure 9. Vertical cross section composites of (a) TC, (b) THL, (c) MS (TLO(ML) and TLO(MD)), (d) TLO and TD, (e) STLC(SS), and (f) PL(PLTLC)-labeled LPS nodes. Dark pink dashed lines are contours of cyclonic potential vorticity (PVU), and black contours are potential temperature (K). The TC, MS, STLC, and PL composites are each based on 1000 randomly chosen nodes tagged with the specific type of label in the specific type of LPS track (i.e., 1000 TC-labeled nodes in TC-labeled tracks). The TLO/TD composite is based on 1000 randomly chosen nodes labeled "TLO" or "TD", except for those in MS or QS tracks. The THL composite is based on 1000 randomly chosen THL-labled nodes.
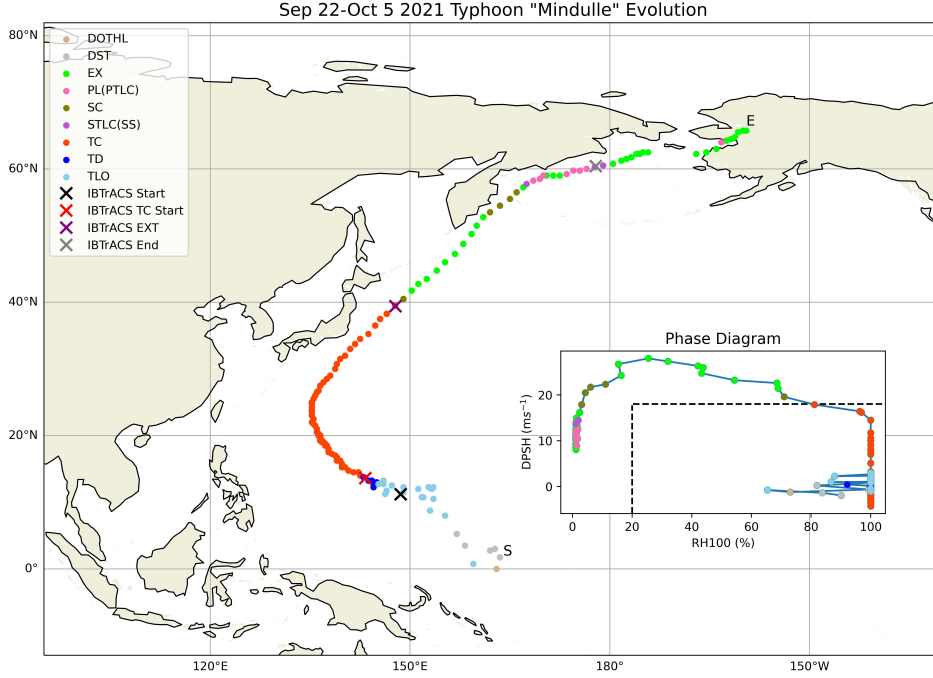
6.2 Other Applications

Figure 10. An example of different LPS labels in a TC (2021 Typhoon "Mindulle") lifetime. The phase diagram shows its evolution on the RH100-DPSH coordinate with the tropical condition threshold outlined in dashed lines. We convert all instances of supersaturation of RH100 to 100% in the phase diagram. S and E indicates the start and the end of the track. The cross marks indicate the position of the start of IBTrACS record (black), the first IBTrACS TC record (red), IBTrACS EXT completion (purple), and the end of IBTrACS record (gray).

We now show some simple applications based on the classified catalog produced by SyCLoPS. One major benefit of SyCLoPS is that it can reveal a fairly complete history of each LPS track, so that the evolution of an LPS can be effectively traced. Thus, a useful application is showing a track along with its labeled nodes, such as the example in Figure 10. The example depicts the track history of the WNP typhoon Mindulle in 2021. Mindulle is first detected as a disturbance near the equator, then gradually intensifies as a non-MS TLO/TD before it becomes stably labeled as TCs. It completed its EXT around 40° N and later develops into a STLC and PL before dissipating as a EX in Alaska. The genesis time (the first TD label time), the first TC record time, and the EXT completion time are all within 12-hours of the corresponding IBTrACS records, while the record given by SyCLoPS further extends the IBTrACS track length. A phase diagram displayed by the DPSH-RH100 coordinate is attached to the figure. The phase evolution shows that the RH100 of the TC stays at a high level while the environmental wind shear gradually increases. The system's RH100 decreases sharply during EXT, which is completed when the TC no longer satisfied the DPSH criteria from the tropical condition. In its final stage, the system enters a lower-sheared environment with very low RH100. More examples like this of different LPS classes (including North Atlantic hurricanes, the "Duck", an MS, and TLCs) can be found in Figs. S7-9 in SI.

The labeled nodes can also be combined with the LPS size blobs we generated when computing LOWSIZE to derive the accumulated integrated kinetic energy (IKE; Powell & Reinhold, 2007) of targeted LPSs. SI Fig. S6 shows an illustration of the labeled
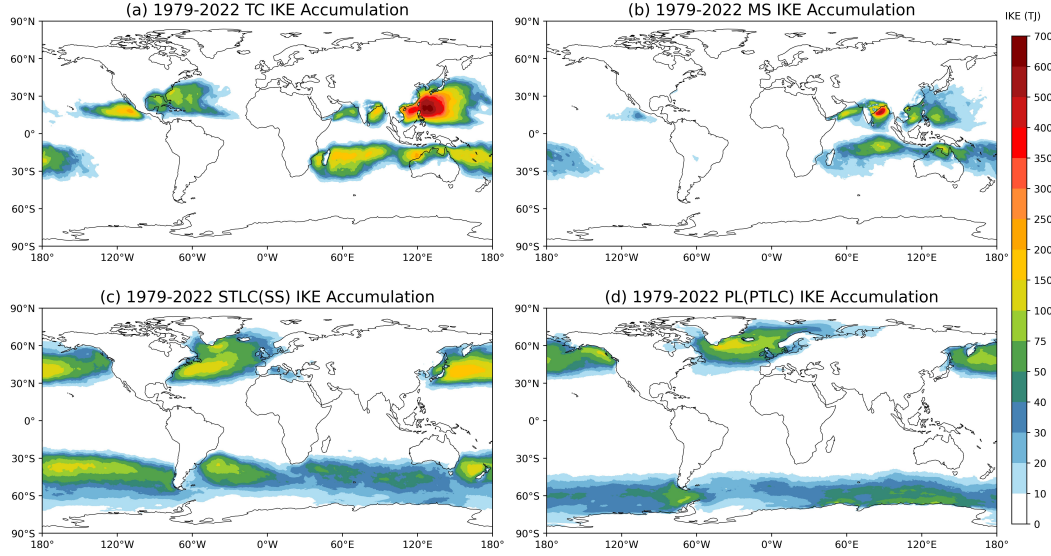
Figure 11. IKE of (a) TC, (b) MS, (c) STLC(SS), and (d) PL(PTLC) accumulated over the 1979-2022 period.

LPS size blobs. IKE is directly correlated with the potential destructiveness of LPSs, as it takes the size parameter into account. The IKE of an LPS is defined as the 1 m-deep mean kinetic energy at the surface level (here approximated by the 925 hPa level) within the LPS extent we define for LOWSIZE. Accumulated IKE of an LPS can be useful to study trends in LPS activity (Kreussler et al., 2021). In Figure 11, we show the accumulated IKE (in trillion joules, TJ) of the four types of high-impact LPS nodes from 1979 to 2022. Specifically, we select blobs associated with TCs (TC nodes) in TC-labeled tracks, all (MS and non-MS) TDs and TLOs in MS-labeled tracks, STLCs in STLC-labeled tracks, and PLs in PL-labeled tracks are selected, respectively, for their IKE accumulations. The results indicate that TCs have the most widespread and severe wind impact over land, while the kinetic energy of MSs accumulates the most along the coast of the Bay of Bengal. STLCs are kinetically active in several hotspots globally. The influence from their winds extends to places including the east coast of the United States, southeast Australia and New Zealand, southern Chile, northern Japan, and the Mediterranean coasts, among other. Besides the Antarctic region, PLs pose the greatest threats to the coasts of the Nordic Seas and the Gulf of Alaska. IKE's spatial distribution patterns may appear different from the LPS frequencies because IKE is storm size-sensitive. For example, even though high TC frequencies are found concentrated in the Eastern Pacific basin (Fig. 8a), TC IKE is far more prominent in the WNP basin due to its largest mean observed TC size among all major basins (Chavas & Emanuel, 2010). Similarly, IKE for STLC in the Mediterranean Sea appear much smaller compared to other hotspots like the WNP and the northwest Atlantic, as TLCs in an open ocean basin can be relatively larger without topographic constraints. Those larger TLCs can possibly be embedded TLCs or "twin-cyclones" like the one shown in SI Fig. S4, and their existence is documented in many case studies in the two basins (e.g., Yamamoto, 2012; Fu et al., 2018; Yokoyama & Yamamoto, 2019).

Objectively tracked LPSs are often used in fractional precipitation contribution studies to tease out the contribution of each LPS type to the total precipitation (e.g., Prat & Nelson, 2013; Prein et al., 2023). The outputs from our framework could be a good source for this purpose, as precipitation blobs can be derived and labeled in a similar manner as for the size blob. Blobs (areas) that satisfy the smoothed 850 hPa CRV thresh-

old (CRV>2×10^{-5} s^{-1}) and a minimum 3-hourly total precipitation threshold of 0.3 mm per 3 hours (0.1 mm hr^{-1}) are highlighted as LPS-associated precipitation and tagged with LPS labels (see SI Fig. S6). We consider this dynamic precipitation detection method more flexible than a fixed or uniform radius method that was often implemented in previous studies (e.g., Dare et al., 2012; Stansfield et al., 2020). We select each class of high-impact LPS nodes and their associated precipitation blobs in the same way as we do for IKE. We demonstrate the fractional contribution of precipitation from the four types of high-impact LPS nodes in Figure 12. The results suggest that TCs contribute over 40% of total precipitation along the coasts of northwestern Australia and south of Baja California. MSs are responsible for a larger fraction of total precipitation than TCs throughout South Asia and inland China. STLCs make up about 5% of total precipitation along the coastal region of the Mediterranean Sea and about 6-7% near northern Japan and the coasts along the Japan Sea. PLs are responsible for several percent of total precipitation in the United Kingdom, northern Europe, and along the coast of Alaska. Since TLCs are active in the winter season, one may expect heavy snowfall as the form of their precipitation.
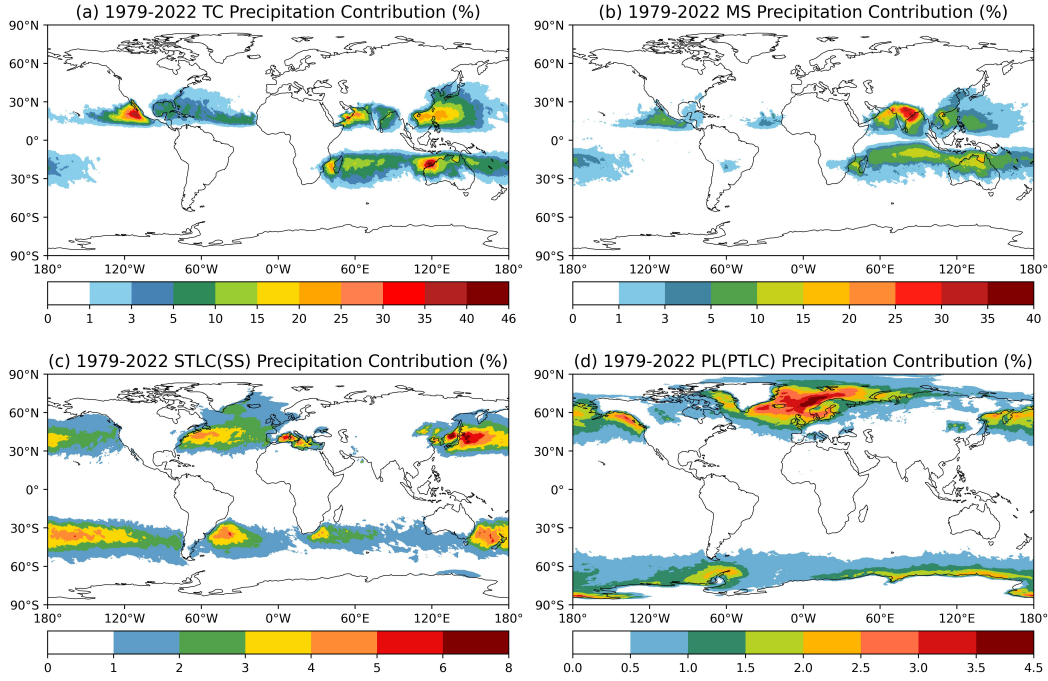

Figure 12. Fractional precipitation contributions from (a) TC, (b) MS, (c) STLC(SS), and (d) PL(PTLC) for the 1979-2022 period.

7 Final Remarks

In this study, we propose an all-in-one detection and classification framework that combines multiple sole-purpose LPS detectors which we refer to as the System for Classification of Low-Pressure Systems (SyCLoPS). SyCLoPS is developed atop the TempestExtremes software package. It is tuned and subsequently applied to the ERA5 reanalysis. To the authors' best knowledge, this work represents the first attempt to classify all LPSs in a single global dataset. Because a single intuitive workflow is employed, no LPS node is repeated or doubly classified. No topographical, latitudinal, or temporal restrictions need to be applied in order to use this framework, and the detection thresh-

old is low enough to include very weak LPS nodes in the detected LPS tracks. As a result, a much more complete LPS lifecycle can be obtained for each LPS track, and its phase evolution can be traced using the labeled nodes. Our results show that the unified framework improves upon previous TC detection skill in TE by both increasing HR and lowering FAR. Detection skill for MSs is comparable to the previous study. SyCLoPS also features the first global TLC system detection. Upon comparing the labels given SyCLoPS to corresponding IBTrACS labels, we observe that SyCLoPS can reasonably label the LPS status in different stages of a TC. We also demonstrate that the resulting classified catalog can be used to study the annual frequencies, vertical cross section composites, track evolution, IKE accumulation, and fractional precipitation contribution of each LPS class. These potential applications could be valuable if applied to climate model outputs to investigate the effects of climate change. SyCLoPS may also be applicable in real-time operations and weather model outputs.

With the classified catalog, the parameter outputs, and the provided software codes, users may personalize the framework to meet their own needs. For example, the detection procedure for a single type of LPS in a given dataset can be easily isolated following a single path from the workflow. More LPS sub-classes may be derived from the provided data and the detection of other atmospheric features. For example, weaker tropical LPSs may be separated into different classes by matching them to distinct tropical wave systems, and polar lows may be divided into those that develop in a front-shear environment versus a reverse-shear environment. Users may also modify the TE specifications and classification conditions to optimize detection under alternate definitions of some LPS classes.

There are some limitations in SyCLoPS worth noting. Firstly, we have only applied SyCLoPS to the global ERA5 dataset, so the thresholds and parameter choices could be biased if applied directly to another global or regional dataset. While we have proposed some suggestions that would enable SyCLoPS's adaptation to different datasets, more fine-tuning in the detection and classification processes may be required. It should also be noted that a dataset with a resolution coarser than ERA5 may be insufficient for detection and classification of smaller features such as early-stage TCs and TLCs. Second, although SyCLoPS features detection and classification of LPSs over any terrain, signals in MSLP or any low-level atmospheric fields can be distorted by elevated topography. Detection over or near those regions are subject to greater errors especially for weak systems. Third, ultimately, the hard cut-off threshold we impose between LPS phases is somewhat arbitrary: namely, there is always a gray zone or transition zone when it comes to the thresholds for a given LPS. Nonetheless, objective LPS detection and classification reduces biases introduced by human error and subjectivity because an objective standard can be strictly followed. However, by nature an LPS can exist in an "impure" and somewhat ambiguous state, which is contrary to fixed thresholds. This conflict is most obvious when a detected LPS persists at the edge of our defined thresholds, leading to its classification jumping between two labels. And lastly, confidence in detecting and classifying global TLC systems is still low due to a lack of global observations. The method for calculating LPS size in TE as described in Appendix C for classifying TLCs can be further improved to more accurately represent the size of a smaller TLC in a larger circulation or the background flow. We expect that there will be other deficiencies discovered and questions raised in the practical use of this experimental framework. Hence, we aim to address some of these remaining issues and evolve the algorithms for future versions of this framework.

Appendix A Catalog Column Documentation

Table A1 is the column documentation of the input (the upper portion) and the classified (the lower portion) LPS catalogs of SyCLoPS. Repeated column names for the classified catalog are skipped.

Table A1. Column Documentation

Column	Unit	Description
TID	-	LPS track ID (0-based) of the input and the output catalog
ISOTIME	-	The UTC timestamp (datetime) of the node
LAT	°	Latitude of the LPS in both the input and the output catalog
LON	°	Longitude of the LPS in both the input and the output catalog
MSLP	Pa	Minimum mean sea level pressure of the system
CMSLCC	Pa	Greatest positive closed contour delta of MSLP over a 2.0° GCD (the core of an LPS)
MSLCC	Pa	Greatest positive closed contour delta of MSLP over a 5.5° GCD
DPSH	$\mathrm{m\,s^{-1}}$	Mean deep-layer wind speed shear between 200 hPa and 850 hPa over a 10.0° GCD
UPTKCC	$\mathrm{m^2\,s^{-2}}$	Greatest negative closed contour delta of the upper-level thickness between 300 hPa and 500 hPa over a 6.5° GCD, referenced to the minimum value within 1.0° GCD
MIDTKCC	$\mathrm{m^2\,s^{-2}}$	Greatest negative closed contour delta of the middle-level thickness between 500 hPa and 700 hPa over a 3.5° GCD, referenced to the minimum value within 1.0° GCD
LOTKCC[a]	$\mathrm{m^2\,s^{-2}}$	Greatest negative closed contour delta of the lower-level thickness between 700 hPa and 925 hPa over a 3.5° GCD, referenced to the minimum value within 1.0° GCD
Z500CC	$\mathrm{m^2\,s^{-2}}$	Greatest positive closed contour delta of geopotential at 500 hPa over a 3.5° GCD referenced to the minimum value within 1.0° GCD
VOR500	$\mathrm{s^{-1}}$	Mean relative vorticity over a 2.5° GCD
RH100	%	Maximum relative humidity at 100 hPa within 2.5° GCD
RHAG850	%	Mean relative humidity over a 2.5° GCD at 850 hPa
T850	K	Air temperature at 850 hPa at the node
Z850	$\mathrm{m^2\,s^{-2}}$	Geopotential at 850 hPa at the node
ZS	$\mathrm{m^2\,s^{-2}}$	Geopotential at the surface at the node
UDF850	$\mathrm{m\,s^{-1}\,sr}$	Difference between the weighted area mean of positive and negative values of 850 hPa U-component wind over a 5.5° GCD
PMX200	$\mathrm{m\,s^{-1}}$	Maximum poleward value of 200 hPa wind speed within 1.0° GCD longitude
LOWSIZE	$\mathrm{km^2}$	The adjusted defined size of the LPS at the current time step
WS	$\mathrm{m\,s^{-1}}$	Maximum wind speed at the 10-m level within 2.0° GCD
Short_Label	-	The abbreviation of the Full_Label
Full_Label	-	The full label name of the LPS based on the classification
Tropical_Flag	-	1 if the LPS is designated as a tropical system, otherwise 0
Transion_Zone	-	1 if the LPS is in the defined transition zone, otherwise 0
Track_Info	-	"TC", "MS", "STLC", "PL", "QS" denoted for TC, MS, STLC, PL, and QS tracks; "EXT", "TT" denoted for EXT and TT completion node
RAWSIZE	$\mathrm{km^2}$	The raw defined size of the LPS at the current time step
IKE	TJ	The integrated kinetic energy computed based on RAW-SIZE's extent (LPS size blob)

[a] 925 hPa may be replaced by 850 hPa if data at this level is scattered in some datasets.

Appendix B Condition List

Table B1. Classification Conditions

Condition Name	Conditions
High-altitude Condition[a]	Z850<ZS
Dryness Condition	RHAG850<60%
Cyclonic Condition	VOR500$\geq$0 s^{-1} if LAT$\geq$0°; VOR500<0 s^{-1} if LAT<0°
Tropical Condition	RH100>20%; DPSH<18 m s^{-1}; T850>280 K
Transition Condition	Tropical Conditon=True; DPSH>10 m s^{-1} or RH100<50%
TC Condition	CMSLCC>215 Pa; LOTKCC<0 m^2 s^{-2}; UPTKCC<-147 m^2 s^{-2}
TD Condition	MSLCC>160 Pa; UPTKCC<0 m^2 s^{-2}
MS Condition	UDF850>0 m s^{-1} ; RHAG850>85%
TLC Condition[b]	CMSLCC>190 Pa; MIDTKCC<0 m^2 s^{-2}; LOTKCC<0 m^2 s^{-2}; (LOWSIZE<5.5 $\times$ 10^5 km^2; LOWSIZE>0 km^2) or (CMSLCC>420 Pa; CMSLCC/MSLCC>0.5)
SC Condition	LOTKCC<0 m^2 s^{-2}; Z500CC>0 m^2 s^{-2}; PMX200[c]>30 m s^{-1}
TC Track Condition	At least 8 TC-labeled nodes in an LPS track
MS Track Condition	At least 10 TLO(ML) or TD(MD)-labeled nodes in an LPS track
STLC Track Condition	At least 2 TLC-labeled nodes (STLC(SS) or PL(PTLC)) and 1 STLC-labeled node in an LPS track
PL Track Condition	At least 2 TLC-labeled nodes (STLC(SS) or PL(PTLC)) and 1 PL-labeled node in an LPS track
QS Track Condition	See SI text S3 for details

[a] It can be simply checking Z850 data availability (null or not) in some datasets.

[b] See Sec. 5.3 for a potential alternative.

[c] PMX200 thresholds used in this framework may be supplemented by other parameters in some regional models. See SI Text S4 for details.

Appendix C LOWSIZE Computation

To calculate LPS size, we refer to the definition of TC size which is typically determined by a TC's outer surface wind radius. We first use TE's `DetectBlobs` to detect blobs (areas) of smoothed 850 hPa cyclonic relative vorticity (CRV) $>2 \times 10^{-5}$ s^{-1} and 925 hPa wind speed >12 m s^{-1}. An alternative condition to this detection requirement is CRV $>4 \times 10^{-5}$ s^{-1} so that TC eyes and EXs' central weaker wind areas can be captured. Wind speed from 925 hPa is used for this calculation, for it is a commonly found lower model level above the surface level. Surface level winds are not used since they can be greatly distorted by complex topography. The 12 m s^{-1} threshold is obtained using a log wind profile from the 8 or 9 m s^{-1} surface outer wind speed threshold often found in TC-size-related studies using ERA5 or climate models(e.g., Stansfield et al., 2020; Bian et al., 2021). The smoothed CRV field is used to control the boundary of an LPS so that the outer wind fields are less likely to connect with an unrelated system nearby. Each detected size blob is then assigned to a detected LPS node if the node is within 5° GCD of the centroid of the blob at the same timestamp, or otherwise within the region bounded by the minimum/maximum latitude/longitude (extent) of the blob. Information on the centroid, extent, and size of each blob can be directly output by TE's `BlobStats`. If multiple nodes are found for one blob, the blob is assigned to the node with the lowest MSLP. Next, the sizes of all the blobs paired with each node are added together as raw LPS sizes. For a quick comparison, the sizes of 2010-2021 WNP TCs computed by our method and the sizes given by the Japan Meteorological Agency (JMA) in IBTrACS have a reasonably high correlation coefficient of 0.63, with very high statistical significance. To avoid misclassifying EXs/SCs as TLCs near shorelines with elevated topography, we adjust the

raw LPS size if the LPS is close to those shorelines with its wind field largely affected by topography. Specifically, we multiply the raw LPS size by two if only 30 to 70% of surface geopoetential within 5° GCD of an LPS is smaller than 7000 $\text{m}^2\,\text{s}^{-2}$ (approximately the 925 hPa level). This adjusted LPS size is defined as LOWSIZE. The non-adjusted (raw) LPS size computed by this method is included as the RAWSIZE column in the classified catalog.

Open Research

The latest version (version 2.2.2) of TempestExtremes (TE) can be installed from `https://github.com/ClimateGlobalChange/tempestextremes` (Ullrich, 2024). The input and the classified catalog created in this study, the shell script for required TE commands, the Python Classifier, the Python script for calculating LOWSIZE, and other useful information about this new framework are all available via the Zenodo repository at `https://doi.org/10.5281/zenodo.10906285`. The ERA5 dataset was obtained from the Research Data Archive at the National Center for Atmospheric Research (`https://doi.org/10.5065/BH6N-5N20`). The IBTrACS archive can be retrieved from `https://www.ncei.noaa.gov/products/international-best-track-archive`. The STARS polar low list (Noer et al., 2011) is available at: `https://projects.met.no/polarlow/stars-dat`. The following two websites were used to evaluate the status of tracked Mediterranean cyclones: `https://meteorologia.uib.eu/medicanes/medicanes_list.html` maintained by the meteorology group of the University of the Balearic Islandsor and `http://medicanes.altervista.org` run by Daniele Bianchino. The objectively tracked easterly wave dataset is downloaded from `https://doi.org/10.17605/OSF.IO/J4HPQ` published by Q. A. Lawton et al. (2022).

Acknowledgments

References

Bernhardt, J. E., & DeGaetano, A. T. (2012). Meteorological factors affecting the speed of movement and related impacts of extratropical cyclones along the us east coast. *Natural hazards*, *61*, 1463–1472.

Bian, G.-F., Nie, G.-Z., & Qiu, X. (2021). How well is outer tropical cyclone size represented in the era5 reanalysis dataset? *Atmospheric Research*, *249*, 105339.

Blackmon, M. L., Wallace, J. M., Lau, N.-C., & Mullen, S. L. (1977). An observational study of the northern hemisphere wintertime circulation. *Journal of the Atmospheric Sciences*, *34*(7), 1040–1053.

Bourdin, S., Fromang, S., Dulac, W., Cattiaux, J., & Chauvin, F. (2022). Intercomparison of four algorithms for detecting tropical cyclones using era5. *Geoscientific Model Development*, *15*(17), 6759–6786.

Cavicchia, L., Dowdy, A., & Walsh, K. (2018). Energetics and dynamics of subtropical australian east coast cyclones: Two contrasting cases. *Monthly Weather Review*, *146*(5), 1511–1525.

Chavas, D. R., & Emanuel, K. A. (2010). A quikscat climatology of tropical cyclone size. *Geophysical Research Letters*, *37*(18).

Dare, R. A., Davidson, N. E., & McBride, J. L. (2012). Tropical cyclone contribution to rainfall over australia. *Monthly Weather Review*, *140*(11), 3606–3619.

Datt, I., Camargo, S. J., Sobel, A. H., McTAGGART-COWAN, R., & Wang, Z. (2022). An investigation of tropical cyclone development pathways as an indicator of extratropical transition. *Journal of the Meteorological Society of Japan. Ser. II*, *100*(4), 707-724.

Emanuel, K. (2005). Genesis and maintenance of" mediterranean hurricanes". *Advances in Geosciences*, *2*, 217–220.

European Centre for Medium-Range Weather Forecasts. (2019, updated monthly). [Dataset]. Research Data Archive at the National Center for Atmospheric Research, Computational and Information Systems Laboratory. Retrieved 2023-01-15, from https://doi.org/10.5065/BH6N-5N20

Evans, J. L., & Braun, A. (2012). A climatology of subtropical cyclones in the south atlantic. *Journal of Climate*, *25*(21), 7328–7340.

Feng, X., Liu, C., Fan, G., Liu, X., & Feng, C. (2016). Climatology and structures of southwest vortices in the ncep climate forecast system reanalysis. *Journal of Climate*, *29*(21), 7675–7701.

Fita, L., Romero, R., Luque, A., Emanuel, K., & Ramis, C. (2007). Analysis of the environments of seven mediterranean tropical-like storms using an axisymmetric, nonhydrostatic, cloud resolving model. *Natural Hazards and Earth System Sciences*, *7*(1), 41–56.

Flaounas, E., Aragão, L., Bernini, L., Dafis, S., Doiteau, B., Flocas, H., ... Ziv, B. (2023). A composite approach to produce reference datasets for extratropical cyclone tracks: application to mediterranean cyclones. *Weather and Climate Dynamics*, *4*(3), 639–661.

Flaounas, E., Davolio, S., Raveh-Rubin, S., Pantillon, F., Miglietta, M. M., Gaertner, M. A., ... others (2022). Mediterranean cyclones: current knowledge and open questions on dynamics, prediction, climatology and impacts. *Weather and Climate Dynamics*, *3*, 173–208.

Fu, S.-M., Sun, J.-H., Li, W.-L., & Zhang, Y.-C. (2018). Investigating the mechanisms associated with the evolutions of twin extratropical cyclones over the northwest pacific ocean in mid-january 2011. *Journal of Geophysical Research: Atmospheres*, *123*(8), 4088–4109.

Gan, M. A., Kousky, V. E., & Ropelewski, C. F. (2004). The south america monsoon circulation and its relationship to rainfall over west-central brazil. *Journal of climate*, *17*(1), 47–66.

Garde, L. A., Pezza, A. B., & Bye, J. A. T. (2010). Tropical transition of the 2001 australian duck. *Monthly Weather Review*, *138*(6), 2038–2057.

Gozzo, L. F., da Rocha, R. P., Reboita, M. S., & Sugahara, S. (2014). Subtropical cyclones over the southwestern south atlantic: Climatological aspects and case study. *Journal of Climate*, *27*(22), 8543–8562.

Guishard, M. P., Evans, J. L., & Hart, R. E. (2009). Atlantic subtropical storms. part ii: climatology. *Journal of Climate*, *22*(13), 3574–3594.

Han, Y., & Ullrich, P. A. (2024). *The system for classification of low-pressure systems (syclops) dataset (based on era5)* [Dataset]. Zenodo. Retrieved from https://doi.org/10.5281/zenodo.10906285

Hart, R. E. (2003). A cyclone phase space derived from thermal wind and thermal asymmetry. *Monthly weather review*, *131*(4), 585–616.

Heo, K.-Y., & Ha, K.-J. (2008). Snowstorm over the southwestern coast of the korean peninsula associated with the development of mesocyclone over the yellow sea. *Advances in Atmospheric Sciences*, *25*, 765–777.

Hepworth, E., Messori, G., & Vichi, M. (2022). Association between extreme atmospheric anomalies over antarctic sea ice, southern ocean polar cyclones and atmospheric rivers. *Journal of Geophysical Research: Atmospheres*, *127*(7),

e2021JD036121.

Hersbach, H., Bell, B., Berrisford, P., Hirahara, S., Horányi, A., Muñoz-Sabater, J., ... others (2020). The era5 global reanalysis. *Quarterly Journal of the Royal Meteorological Society*, *146*(730), 1999–2049.

Hodges, K. I. (1994). A general method for tracking analysis and its application to meteorological data. *Monthly Weather Review*, *122*(11), 2573–2586.

Hoinka, K. P., & Castro, M. D. (2003). The iberian peninsula thermal low. *Quarterly Journal of the Royal Meteorological Society: A journal of the atmospheric sciences, applied meteorology and physical oceanography*, *129*(590), 1491–1511.

Holland, G. J., Lynch, A. H., & Leslie, L. M. (1987). Australian east-coast cyclones. part i: Synoptic overview and case study. *Monthly Weather Review*, *115*(12), 3024–3036.

Hunt, K. M., Turner, A. G., Inness, P. M., Parker, D. E., & Levine, R. C. (2016). On the structure and dynamics of indian monsoon depressions. *Monthly Weather Review*, *144*(9), 3391–3416.

Hurley, J. V., & Boos, W. R. (2015). A global climatology of monsoon low-pressure systems. *Quarterly Journal of the Royal Meteorological Society*, *141*(689), 1049–1064.

Iwao, K., Inatsu, M., & Kimoto, M. (2012). Recent changes in explosively developing extratropical cyclones over the winter northwestern pacific. *Journal of Climate*, *25*(20), 7282–7296.

Knapp, K. R., Diamond, H. J., Kossin, J. P., Kruk, M. C., & Schreck, C. J. (2018). *International best track archive for climate stewardship (ibtracs) project, version 4* [Dataset]. NOAA National Centers for Environmental Information. Retrieved 2023-09-21, from `https://doi.org/10.25921/82ty-9e16`

Knapp, K. R., Kruk, M. C., Levinson, D. H., Diamond, H. J., & Neumann, C. J. (2010). The international best track archive for climate stewardship (ibtracs) unifying tropical cyclone data. *Bulletin of the American Meteorological Society*, *91*(3), 363–376.

Koch, P., Wernli, H., & Davies, H. C. (2006). An event-based jet-stream climatology and typology. *International Journal of Climatology: A Journal of the Royal Meteorological Society*, *26*(3), 283–301.

Kreussler, P., Caron, L.-P., Wild, S., Loosveldt Tomas, S., Chauvin, F., Moine, M.-P., ... others (2021). Tropical cyclone integrated kinetic energy in an ensemble of highresmip simulations. *Geophysical research letters*, *48*(5), e2020GL090963.

Landsea, C. W., & Franklin, J. L. (2013). Atlantic hurricane database uncertainty and presentation of a new database format. *Monthly Weather Review*, *141*(10), 3576–3592.

Lawton, Q., & Majumdar, S. (2018). *Objective tracking of african easterly waves in reanalysis data (updated through 2022)* [Dataset]. OSF. Retrieved from `https://doi.org/10.17605/OSF.IO/J4HPQ`

Lawton, Q. A., Majumdar, S. J., Dotterer, K., Thorncroft, C., & Schreck III, C. J. (2022). The influence of convectively coupled kelvin waves on african easterly waves in a wave-following framework. *Monthly weather review*, *150*(8), 2055–2072.

Li, J., & Zeng, Q. (2003). A new monsoon index and the geographical distribution of the global monsoons. *Advances in atmospheric sciences*, *20*, 299–302.

Li, L., Zhang, R., Wen, M., Duan, J., & Qi, Y. (2019). Characteristics of the tibetan plateau vortices and the related large-scale circulations causing different precipitation intensity. *Theoretical and Applied Climatology*, *138*, 849–860.

Lodise, J., Merrifield, S., Collins, C., Rogowski, P., Behrens, J., & Terrill, E. (2022). Global climatology of extratropical cyclones from a new tracking approach and associated wave heights from satellite radar altimeter. *Journal of Geophysical Research: Oceans*, *127*(11), e2022JC018925.

Lu, J., & Ding, Y. (1989). Climatic study on the summer tropical easterly jet at 200 hpa. *Advances in atmospheric sciences*, *6*(2), 215–226.

Montgomery, M. T., & Farrell, B. F. (1992). Polar low dynamics. *Journal of the atmospheric sciences*, *49*(24), 2484–2505.

Moreno-Ibáñez, M., Laprise, R., & Gachon, P. (2021). Recent advances in polar low research: Current knowledge, challenges and future perspectives. *Tellus A: Dynamic Meteorology and Oceanography*, *73*(1), 1–31.

Neu, U., Akperov, M. G., Bellenbaum, N., Benestad, R., Blender, R., Caballero, R., ... others (2013). Imilast: A community effort to intercompare extratropical cyclone detection and tracking algorithms. *Bulletin of the American Meteorological Society*, *94*(4), 529–547.

NHC. (n.d.). *USA glossary of features.* Retrieved 2023-12-02, from `https://www.nhc.noaa.gov/marine/docs/USA_Glossary.pdf`

Noer, G., Saetra, Ø., Lien, T., & Gusdal, Y. (2011). A climatological study of polar lows in the nordic seas. *Quarterly Journal of the Royal Meteorological Society*, *137*(660), 1762–1772.

Nordeng, T. E., & Rasmussen, E. A. (1992). A most beautiful polar low. a case study of a polar low development in the bear island region. *Tellus A*, *44*(2), 81–99.

Poveda, G., Jaramillo, L., & Vallejo, L. F. (2014). Seasonal precipitation patterns along pathways of south american low-level jets and aerial rivers. *Water Resources Research*, *50*(1), 98–118.

Powell, M. D., & Reinhold, T. A. (2007). Tropical cyclone destructive potential by integrated kinetic energy. *Bulletin of the American Meteorological Society*, *88*(4), 513–526.

Prat, O. P., & Nelson, B. R. (2013). Mapping the world's tropical cyclone rainfall contribution over land using the trmm multi-satellite precipitation analysis. *Water Resources Research*, *49*(11), 7236–7254.

Prein, A. F., Mooney, P. A., & Done, J. M. (2023). The multi-scale interactions of atmospheric phenomenon in mean and extreme precipitation. *Earth's Future*, *11*(11), e2023EF003534.

Pytharoulis, I., Craig, G. C., & Ballard, S. P. (2000). The hurricane-like mediterranean cyclone of january 1995. *Meteorological Applications: A journal of forecasting, practical applications, training techniques and modelling*, *7*(3), 261–279.

Qian, W., & Lee, D.-K. (2000). Seasonal march of asian summer monsoon. *International Journal of Climatology: A Journal of the Royal Meteorological Society*, *20*(11), 1371–1386.

Rasmussen, E. A., & Turner, J. (2003). *Mesoscale weather systems in the polar regions.* Cambridge University Press.

Reed, R. J., Norquist, D. C., & Recker, E. E. (1977). The structure and properties of african wave disturbances as observed during phase iii of gate. *Monthly Weather Review*, *105*(3), 317–333.

Reeder, M. J., Smith, R. K., Deslandes, R., Tapper, N. J., & Mills, G. A. (2000). Subtropical fronts observed during the 1996 central australian fronts experiment. *Australian Meteorological Magazine*, *49*(3), 181–200.

Roberts, M. J., Camp, J., Seddon, J., Vidale, P. L., Hodges, K., Vanniere, B., ... others (2020). Impact of model resolution on tropical cyclone simulation using the highresmip–primavera multimodel ensemble. *Journal of Climate*, *33*(7), 2557–2583.

Roberts, M. J., Camp, J., Seddon, J., Vidale, P. L., Hodges, K., Vannière, B., ... others (2020). Projected future changes in tropical cyclones using the cmip6 highresmip multimodel ensemble. *Geophysical research letters*, *47*(14), e2020GL088662.

Romero, R., & Emanuel, K. (2017). Climate change and hurricane-like extratropical

cyclones: Projections for north atlantic polar lows and medicanes based on cmip5 models. *Journal of Climate*, *30*(1), 279–299.

Schreck, C. J., Knapp, K. R., & Kossin, J. P. (2014). The impact of best track discrepancies on global tropical cyclone climatologies using ibtracs. *Monthly Weather Review*, *142*(10), 3881–3899.

Schultz, D. M., & Keyser, D. (2021). Antecedents for the shapiro–keyser cyclone model in the bergen school literature. *Bulletin of the American Meteorological Society*, *102*(2), E383–E398.

Shimada, U., Wada, A., Yamazaki, K., & Kitabatake, N. (2014). Roles of an upper-level cold vortex and low-level baroclinicity in the development of polar lows over the sea of japan. *Tellus A: Dynamic Meteorology and Oceanography*, *66*(1), 24694.

Sikka, D. R. (2006). *A study on the monsoon low pressure systems over the Indian region and their relationship with drought and excess monsoon seasonal rainfall* (No. 217). Center for OceanLandAtmosphere Studies.

Smith, E. A. (1986). The structure of the arabian heat low. part i: Surface energy budget. *Monthly weather review*, *114*(6), 1067–1083.

Spengler, T., Reeder, M. J., & Smith, R. K. (2005). The dynamics of heat lows in simple background flows. *Quarterly Journal of the Royal Meteorological Society*, *131*(612), 3147–3165.

Stansfield, A. M., & Reed, K. A. (2021). Tropical cyclone precipitation response to surface warming in aquaplanet simulations with uniform thermal forcing. *Journal of Geophysical Research: Atmospheres*, *126*(24), e2021JD035197.

Stansfield, A. M., Reed, K. A., Zarzycki, C. M., Ullrich, P. A., & Chavas, D. R. (2020). Assessing tropical cyclones contribution to precipitation over the eastern united states and sensitivity to the variable-resolution domain extent. *Journal of Hydrometeorology*, *21*(7), 1425–1445.

Stoll, P. J. (2022). A global climatology of polar lows investigated for local differences and wind-shear environments. *Weather and Climate Dynamics*, *3*(2), 483–504.

Stoll, P. J., Graversen, R. G., Noer, G., & Hodges, K. (2018). An objective global climatology of polar lows based on reanalysis data. *Quarterly Journal of the Royal Meteorological Society*, *144*(716), 2099–2117.

Terpstra, A., Michel, C., & Spengler, T. (2016). Forward and reverse shear environments during polar low genesis over the northeast atlantic. *Monthly Weather Review*, *144*(4), 1341–1354.

Toomey, T., Amores, A., Marcos, M., Orfila, A., & Romero, R. (2022). Coastal hazards of tropical-like cyclones over the mediterranean sea. *Journal of Geophysical Research: Oceans*, *127*(2), e2021JC017964.

Tucker, D. F. (1999). The summer plateau low pressure system of mexico. *Journal of climate*, *12*(4), 1002–1015.

Ullrich, P. A. (2024). *Tempestextremes github repository* [Software]. GitHub. Retrieved 2024-03-29, from `https://github.com/ClimateGlobalChange/tempestextremes`

Ullrich, P. A., & Zarzycki, C. M. (2017). Tempestextremes: A framework for scale-insensitive pointwise feature tracking on unstructured grids. *Geoscientific Model Development*, *10*(3), 1069–1090.

Ullrich, P. A., Zarzycki, C. M., McClenny, E. E., Pinheiro, M. C., Stansfield, A. M., & Reed, K. A. (2021). Tempestextremes v2. 1: A community framework for feature detection, tracking and analysis in large datasets. *Geoscientific model development discussions*, *2021*, 1–37.

U.S. Navy. (1994). *Local area forecasters handbook for Naval Air Station Bermuda*. Naval Atlantic Meteorology Facility, Bermuda.

Vishnu, S., Boos, W., Ullrich, P., & O'brien, T. (2020). Assessing historical variabil-

ity of south asian monsoon lows and depressions with an optimized tracking algorithm. *Journal of Geophysical Research: Atmospheres*, *125*(15), e2020JD032977.

Winckler, P., Contreras-López, M., Campos-Caba, R., Beyá, J. F., & Molina, M. (2017). El temporal del 8 de agosto de 2015 en las regiones de valparaíso y coquimbo, chile central. *Latin american journal of aquatic research*, *45*(4), 622–648.

Yamamoto, M. (2012). Rapid merger and recyclogenesis of twin extratropical cyclones leading to heavy precipitation around japan on 9–10 october 2001. *Meteorological Applications*, *19*(1), 36–53.

Yokoyama, Y., & Yamamoto, M. (2019). Influences of surface heat flux on twin cyclone structure during their explosive development over the east asian marginal seas on 23 january 2008. *Weather and Climate Extremes*, *23*, 100198.

Zappa, G., Shaffrey, L., & Hodges, K. (2014). Can polar lows be objectively identified and tracked in the ecmwf operational analysis and the era-interim reanalysis? *Monthly Weather Review*, *142*(8), 2596–2608.

Zarzycki, C. M., & Ullrich, P. A. (2017). Assessing sensitivities in algorithmic detection of tropical cyclones in climate data. *Geophysical Research Letters*, *44*(2), 1141–1149.

Zhang, W., Villarini, G., Scoccimarro, E., & Napolitano, F. (2021). Examining the precipitation associated with medicanes in the high-resolution era-5 reanalysis data. *International Journal of Climatology*, *41*, E126–E132.